Self-Assembled Dinuclear Lanthanide Helicates: Substantial Luminescence Enhancement upon Replacing Terminal Benzimidazole Groups by Carboxamide Binding Units

Noreen Martin,[†] Jean-Claude G. Bünzli,*[,†] Vickie McKee,[‡] Claude Piguet,*[,§] and Gérard Hopfgartner[⊥]

Institute of Inorganic and Analytical Chemistry, University of Lausanne, CH-1015 Lausanne, Switzerland, Department of Inorganic Chemistry, Queen's University, BT9 5AG, Belfast, N. Ireland, Department of Inorganic, Analytical and Applied Chemistry, University of Geneva, CH-1211 Geneva 4, Switzerland, and Pharma Division, F. Hoffmann-La Roche Ltd., CH-4070 Basle, Switzerland

Received November 6, 1997

The segmental ligands bis{1-alkyl-2-[6′-(*N*,*N*-diethylcarbamoyl)pyridin-2′-yl]benzimidazol-5-yl}methane (alkyl = methyl (L^5), ethyl (L^6)) react with lanthanide perchlorates (Ln = La, Eu, Gd, Tb) in acetonitrile to yield the f−f dinuclear homotopic triple-stranded helicates $[Ln_2(L^i)_3]^{6+}$ (i = 5, 6) under thermodynamic control. The crystal structure of $[Tb_2(L^6)_3](ClO_4)_3(MeCN)_2(THF)_{0.5}(EtOH)_{0.5}$ (**11a**, $C_{124}H_{145}N_{26}O_{31}Cl_6Tb_2$, triclinic, $P\bar{1}$, Z = 2) shows the wrapping of the ligands about a pseudo-C_3 axis passing through the metal ions. The Tb ions are 9-coordinate in facial pseudo-tricapped trigonal prismatic sites and are separated by 9.06 Å. ^{1}H-NMR and ES-MS data establish that the triple helical structure is maintained in solution. Spectrophotometric titrations (Ln = La, Eu) indicate log β_{23} = 24−25 and the formation of a 2:2 complex $[Ln_2(L^5)_2]^{6+}$ (log β_{22} = 19−20). Quantum yield determination in acetonitrile shows that the terminal *N*,*N*-diethylcarboxamide groups in L^5 favor efficient intramolecular $L^5 \rightarrow$ Eu(III) energy transfers leading to strong Eu-centered red luminescence, 50 times as intense as the luminescence observed when the carboxamide groups are replaced by substituted benzimidazole units in $[Eu_2(L^4)_3]^{6+}$. Resistance toward hydrolysis also results from the use of carboxamide groups, and no quenching of luminescence is observed for $[Eu_2(L^5)_3]^{6+}$ in moist acetonitrile up to 2.5 M water. The crucial role played by carboxamide groups for the control of structural, electronic, and photophysical properties is discussed. Replacing perchlorates by triflates allows the isolation of the dinuclear double-stranded helicate $[Eu_2(L^6)_2(CF_3SO_3)_4(H_2O_2)_2](CF_3SO_3)_2(MeOH)_2(H_2O)_{5.5}$, whose crystal structure (**13a**, $C_{85}H_{106}Eu_2F_{18}N_{16}O_{30}S_6$, monoclinic, $C2/m$, Z = 2) reveals a side-by-side arrangement of the two strands and 9-coordinate Eu ions linked through hydrogen-bonded water molecules.

Introduction

Lanthanide-containing luminescent stains[1] are gaining significance in view of their applications in biomedical analyses,[2] fluorescence imaging,[2] and, possibly, cancer phototherapy.[3] Preorganized receptors which encapsulate the luminescent Eu(III) and Tb(III) ions to protect their excited states against deexcitation through solvent interaction are also used in other biomedical applications as contrast agents for magnetic resonance imaging,[4] as catalysts in RNA hydrolysis,[5] or in cancer radiotherapy.[6] Both mono- and dinuclear complexes are used, and our interest lies in the latter because they are adequate models to study intramolecular metal-to-metal energy transfer pathways in addition to providing two probe signals in one stain. The design of organized molecular architectures containing lanthanide ions is therefore a theme of considerable current interest in supramolecular chemistry.[7] However, the selective introduction of Ln(III) ions into edifices with specific coordination sites and predetermined photophysical properties represents a synthetic challenge[8] since these ions display large and variable coordination numbers with little stereochemical preferences.[9] Macrocyclic and macrobicyclic compartmental ligands have been systematically investigated for the preparation of mono- and polynuclear lanthanide complexes,[10,11] but improved structural control and protection of Ln(III) ions is obtained with

[†] University of Lausanne.
[‡] Queen's University.
[§] University of Geneva.
[⊥] F. Hoffmann-La Roche Ltd.

(1) Bünzli, J.-C. G. In *Lanthanide Probes in Life, Chemical and Earth Sciences*; Bünzli, J.-C. G., Choppin, G. R., Eds.; Elsevier Publishing Co: Amsterdam, 1989; Chapter 7.
(2) *Bioanalytical Applications of Labeling Technologies*; Hemmilä, I., Stahlberg, T., Mottram P., Eds.; Wallac Oy: Turku, Finland, 1994.
(3) Sessler, J. L.; Kral, V; Hoehner, M. C.; Chin, K. O. A.; Davila, R. M. *Pure Appl. Chem.* **1996**, *68*, 1291−1295.
(4) Lauffer, R. B. In *MRI Clinical Magnetic Resonance Imaging*, 2nd ed.; Edelman, R. R., Zlatkin, M. B., Hesselink, J. R., Eds.; W. B. Saunders Co.: Philadelphia, PA, 1996; Vol. 1, Chapter 5.
(5) Bruice, T. C.; Tsubouchi, A; Dempey, R. O.; Olson, L. P. *J. Am. Chem. Soc.* **1996**, *118*, 9867−9875.
(6) DeNardo, G. L.; Mirik, G. R.; Kroger, L. A.; O'Donnel, R. T.; Meares, C. F.; DeNardo, S. J. *J. Nucl. Med.* **1996**, *37*, 451−456.
(7) Lehn, J.-M. *Supramolecular Chemistry, Concepts and Perspectives*; VCH: Weinheim, Germany, 1995. Piguet, C. *Chimia* **1996**, *50*, 144−153. Piguet, C.; Bünzli, J.-C. G. *Eur. J. Solid State Inorg. Chem.* **1996**, *33*, 165−174.
(8) Piguet, C.; Bünzli, J.-C. G.; Bernardinelli, G.; Hopfgartner, G.; Williams, A. F. *J. Alloys Compds.* **1995**, *225*, 324−331.
(9) Bünzli, J.-C. G. In *Basic and Applied Aspects of Rare Earths*; Caro, P., Saez-Puche, R., Eds; Editorial Complutense: Madrid, 1997, in press. Choppin, G. R. In *Lanthanide Probes in Life, Chemical and Earth Sciences*; Bünzli, J.-C. G., Choppin, G. R., Eds.; Elsevier Publishing Co: Amsterdam, 1989; Chapter 1.
(10) Alexander, V. *Chem. Rev.* **1995**, *95*, 273−342 and references therein.

S0020-1669(97)01401-8 CCC: $15.00
Published on Web 01/16/1998

Chart 1

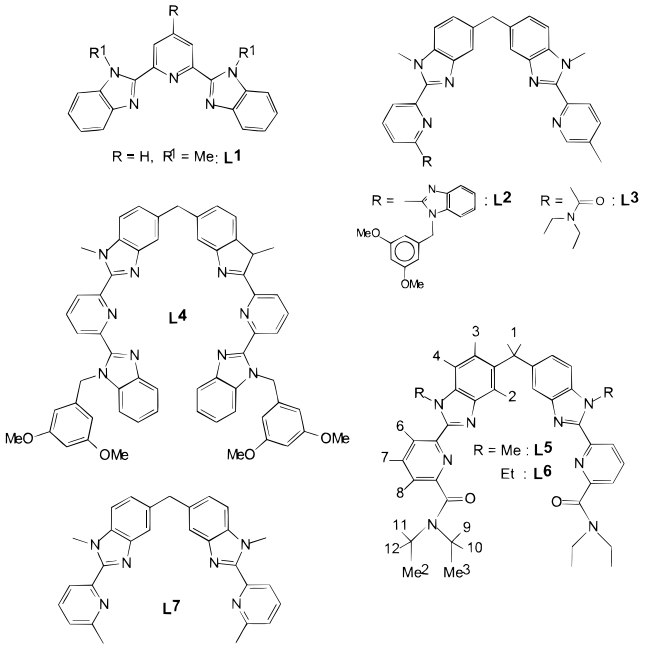

predisposed tri- to hexapodal ligands.[12−15] In our laboratories, we have developed three series of ligands L^{1-4} derived from bis(benzimidazole)pyridine receptors which are able to self-assemble with lanthanide and 3d-transition ions, yielding mononuclear and f−f as well as d−f dinuclear assemblies:[16] (i) The tridentate aromatic ligand L^1 (see Chart 1) leads to triple helical complexes $[Ln(L^1)_3]^{3+}$ displaying sizable $\pi\pi$-stacking interactions[17] in which the structural,[17,18] photophysical,[18,19] and thermodynamic[19] properties can be finely tuned by a judicious choice of the substituents R and R^1. Similarly, the structural and photophysical properties of nitrato complexes $[Ln(NO_3)_3(L^1)(solv)_x]$ may also be adjusted by changing R and R^1.[20,21] (ii) The segmental heterotopic ligand L^2 was designed to prepare d−f noncovalent lanthanide podates $[LnM(L^2)_3]^{5+}$ with M = Fe(II)[22] and Zn(II),[23] the former displaying spin-crossover behavior. The replacement of the terminal substituted benzimidazole moiety on the tridentate side of L^2 by an *N*,*N*-diethylcarbamoyl unit in L^3 improves the selectivity of the self-assembly and favors ligand-to-Eu(III) energy transfer processes in the final complex $[EuZn(L^3)_3]^{5+}$ which is about 10^3 more luminescent than $[EuZn(L^2)_3]^{5+}$,[24] while the Fe(II) spin-state equilibria in $[LnFe(L^3)_3]^{5+}$ can be finely controlled by the size of the coordinated Ln(III) ions.[25] (iii) The homotopic segmental ligand L^4, obtained by linking two bis(benzimidazole)pyridine strands by a methylene bridge, was designed to study Ln(III) → Ln(III) energy transfer processes and to provide dinuclear pseudocylindrical luminescent probes.[7] The homotopic triple-stranded helicate $[Eu_2(L^4)_3]^{6+}$ retains a pseudo-D_3 symmetry both in the solid state and in solution, but it is only weakly luminescent at room temperature and it is very sensitive to water: two severe handicaps for its use as a probe.[26] To avoid these difficulties, the two terminal benzimidazole substituents were replaced by *N*,*N*-diethylcarbamoyl groups to yield $L^{5,6}$. In this paper, we present the synthesis of the new segmental ligands L^5 and L^6 and the thermodynamic assembly processes leading to the strongly luminescent triple-stranded helicates $[Ln_2(L^i)_3]^{6+}$ (i = 5 or 6; Ln = La, Eu, Tb, Gd, Lu). Detailed photophysical studies in the solid state are reported to determine whether the series of complexes is isostructural or not. Attention is also focused on the quantum yields in acetonitrile, on the resistance of the helicates to the addition of water, and on their conversion into the double-stranded helicates $[Ln_2(L^i)_2]^{6+}$ upon the addition of an excess of metal ions.

Experimental Section

Solvents and starting materials were purchased from Fluka AG (Buchs, Switzerland) and used without further purification, unless otherwise stated. Acetonitrile, dichloromethane, *N*,*N*-dimethylformamide (DMF), and triethylamine were distilled from CaH_2; thionyl chloride was distilled from elemental sulfur. Silica gel (Merck 60, 0.04−0.06 mm) was used for preparative column chromatography.

Spectroscopic and Analytical Measurements. Reflectance spectra were recorded as finely ground powders dispersed in MgO (5%) with MgO as the reference on a Perkin-Elmer Lambda 19 spectrometer equipped with a Labsphere RSA-PE-19 integration sphere. Electronic spectra in the UV−vis range were recorded at 20 °C with Perkin-Elmer Lambda 7 spectrometer using 1.0 and 0.1 cm quartz cells. Spectrophotometric titrations were performed on the latter spectrometer connected to an external computer. Typically, 21 samples were prepared 24 h in advance of the spectrophotometric measurement to ensure equilibrium had been reached. Each aliquot had a total L^5 concentration of 10^{-4} M, with a stepwise increment of 0.2 mL of 10^{-5} M $Ln(ClO_4)_3 \cdot xH_2O$ (Ln = La and Eu) solution added over that of the previous sample. The absorbances over 10 different wavelengths were recorded using 0.1 cm quartz cells and transferred to the computer. Plots of molar absorption coefficient as a function of the metal:ligand ratio gave a first indication of the number and stoichiometry of the complexes formed in solution; factor analysis[27] was then applied to the data to confirm the number of absorbing species. Eventually, a model for the distribution of species was fitted with a nonlinear least-

(11) Guerriero, P.; Tamburini, S.; Vigato, P. A. *Coord. Chem. Rev.* **1995**, *139*, 17−243 and references therein.
(12) Yang, L. W.; Liu, S.; Wong, E.; Rettig, S. J.; Orvig, C. *Inorg. Chem.* **1995**, *34*, 2164−2178 and references therein. Caravan, P.; Hedlund, T.; Liu, S.; Sjöberg, S.; Orvig, C. *J. Am. Chem. Soc.* **1995**, *117*, 11230−11238.
(13) Balzani, V.; Berghmans, E.; Lehn, J.-M.; Sabbatini, N.; Terörde, R.; Ziessel, R. *Helv. Chim. Acta* **1990**, *73*, 2083−2089. Ziessel, R.; Maestri, M.; Prodi, L.; Balzani, V.; Van Doersselaer, A. *Inorg. Chem.* **1993**, *32*, 1237−1241. Sabbatini, N.; Guardigli, M.; Manet, I.; Bolleta, F.; Ziessel, R. *Inorg. Chem.* **1994**, *33*, 955−959.
(14) Jones, P. L.; Amoroso, A. J.; Jeffery, J. C.; Mc Cleverty, J. A.; Psillakis, E.; Rees, L. H.; Ward, M. D. *Inorg. Chem.* **1997**, *36*, 10−18.
(15) Xu, J.; Franklin, S. J.; Whisenhunt, D. W.; Raymond, K. N. *J. Am. Chem. Soc.* **1995**, *117*, 7245−7246.
(16) Piguet,C.; Bernardinelli, G.; Hopfgartner, G. *Chem. Rev.* **1997**, *97*, 2005−2062.
(17) Piguet, C.; Bünzli, J.-C. G.; Bernardinelli, G.; Williams, A. F. *Inorg. Chem.* **1993**, *32*, 4139−4149.
(18) Piguet, C.; Bünzli, J.-C. G.; Bernardinelli, G.; Bochet, C. G.; Froidevaux, P. *J. Chem. Soc., Dalton Trans.* **1995**, 83−97.
(19) Bünzli, J.-C. G.; Petoud, S.; Piguet, C.; Renaud, F. J. *Alloys Compds.* **1997**, *249*, 14−24.
(20) Piguet, C.; Williams, A. F.; Bernardinelli, G.; Moret, E.; Bünzli, J.-C. G. *Helv. Chim. Acta* **1992**, *75*, 1697−1717.
(21) Petoud, S.; Bünzli, J.-C. G.; Schenk, K. J.; Piguet, C. *Inorg. Chem.* **1997**, *36*, 1345−1353.
(22) Piguet, C.; Rivara-Minten, E.; Hopfgartner, G.; Bünzli, J.-C. G. *Helv. Chim. Acta* **1995**, *78*, 1651−1672.
(23) Piguet, C.; Rivara-Minten, E.; Hopfgartner, G.; Bünzli, J.-C. G. *Helv. Chim. Acta* **1995**, *78*, 1541−1566. Piguet, C.; Hopfgartner, G.; Williams, A. F.; Bünzli, J.-C. G. *J. Chem. Soc., Chem. Commun.* **1995**, 491−493.
(24) Piguet, C.; Bünzli, J.-C. G.; Bernardinelli, G.; Hopfgartner, G.; Petoud, S.; Schaad, O. *J. Am. Chem. Soc.* **1996**, *118*, 6681−6697. Piguet, C.; Bernardinelli, G.; Bünzli, J.-C. G.; Petoud, S.; Hopfgartner, G. *J. Chem. Soc., Chem. Commun.* **1995**, 2575−2577.
(25) Piguet, C.; Rivara-Minten, E.; Bernardinelli, G.; Bünzli, J.-C. G.; Hopfgartner, G. *J. Chem. Soc., Dalton Trans.* **1997**, 421−433.
(26) Piguet, C.; Bünzli, J.-C. G.; Bernardinelli, G.; Hopfgartner, G.; Williams, A. F. *J. Am. Chem. Soc.* **1993**, *115*, 8197−8206. Bernardinelli, G.; Piguet, C.; Williams, A. F. *Angew. Chem., Int. Ed. Engl.* **1992**, *31*, 1622−1624.
(27) Malinowski, E. R.; Howery, D. G. *Factor Analysis in Chemistry*; J. Wiley: New York, Chichester, Brisbane, and Toronto, 1980.

squares algorithm to give stability constants using the program SPECFIT.[28] IR spectra were obtained from KBr pellets with a Mattson α-Centauri FT-IR spectrometer. ^{1}H-NMR spectra were recorded at 25 °C on a Bruker AM-360 spectrometer. Chemical shifts are reported in parts per million with respect to TMS. Pneumatically-assisted ES-MS spectra were recorded from 10^{-4} M acetonitrile solutions on an API III tandem spectrometer (PE Sciex) by infusion at 4−10 μL/min. The spectra were recorded under low up-front declustering as previously described.[29,30]

The experimental procedures for high-resolution, laser excited luminescence studies have been published previously.[20] Solid-state samples were finely powdered, and low temperature (10 and 77 K) was achieved by means of either a Cryodyne model 22 closed-cycle refrigerator from CTI Cryogenics or an Oxford DN 704 cryostat. Luminescence spectra were corrected for the instrumental function but not the excitation spectra. Lifetimes (τ) are averages of at least 3−5 independent determinations. Quantum yields were determined as previously described[21] from 10^{-3} M solution to avoid decomplexation, but at wavelengths where (i) the Lambert−Beer law is obeyed and (ii) the absorption of the reference $[Ln(terpy)_3]^{3+}$ (Ln = Eu, Tb) closely matches that of the sample. Ligand excitation and emission spectra were recorded on a Perkin-Elmer LS-50B spectrometer equipped for low-temperature (77 K) measurements.

Crystal Data for $[Tb_2(L^6)_3](ClO_4)_6(THF)_{0.5}(MeCN)_2(EtOH)_{0.5}$ (11a): $C_{124}H_{145}Cl_6N_{26}O_{31}Tb_2$, colorless block, dimensions 0.64 × 0.30 × 0.28 mm, triclinic, a = 15.916(2) Å, b = 16.367(2) Å, c = 28.574(4) Å, α = 79.57(1)°, β = 81.76(1)°, γ = 71.54(1)°, V = 6914(2) Å^3, space group $P\bar{1}$, Z = 2, μ = 1.212 mm^{-1}, $F(000)$ = 3102. Unit cell parameters were determined by nonlinear least-squares refinement of 39 reflections ($10 < 2\theta < 25°$). A total of 25 203 reflections were collected in the range $4 < 2\theta < 50°$, crystal stability was monitored by recording 3 check reflections every 100 reflections, and data were corrected for a decay of 4%. Data were corrected for Lorentz and polarization effects, and an empirical absorption correction, based on ψ-scans, was applied (T_{max} = 0.884, T_{min} = 0.774). The structure was solved by direct methods (TREF[31]) and refined by blocked matrix least-squares on F^2, using all 24 243 independent reflections (R_{int} = 0.033). The refinement, on 1676 parameters, converged with wR2 = 0.1833, goodness of fit = 1.061 (all data), and conventional R1 = 0.0648 (2σ data). One of the benzimidazole groups (C(16a)−C(24a)) shows some rotational disorder, and this has been modeled by including a minor (35%) component in a second orientation (N(5x)−C(24x)). A number of the terminal ethyl groups show high atomic displacement parameters, suggesting a degree of disorder, but no attempt has been made to model this. Of the six perchlorate counterions, those centered on Cl(1), Cl(2), Cl(3), and Cl(4) refined without any difficulty. The ions centered on Cl(5) and Cl(6) were disordered and have been modeled as interpenetrating tetrahedra. One half-occupancy THF molecule was located, but the oxygen atom was not identified and all the atoms were refined as carbon. One full-occupancy and two half-occupancy acetonitrile molecules and an ethanol disordered about a center of symmetry complete the structure. All the full-occupancy non-hydrogen atoms have been refined with anisotropic atomic displacement parameters. Hydrogen atoms were inserted at calculated positions on the full-occupancy atoms only.

Crystal Data for $[Eu_2(L^6)_2(CF_3SO_3)_4(H_2O)_2](CF_3SO_3)_2(MeOH)_2(H_2O)_{5.5}$ (13a): $C_{85}H_{106}Eu_2F_{18}N_{16}O_{30}S_6$, colorless block, dimensions 0.43 × 0.40 × 0.20 mm, monoclinic, a = 24.697(3) Å, b = 21.081(3) Å, c = 11.218(2) Å, β = 100.22(1)°, V = 5747(2) Å^{-3}, space group $C2/m$, Z = 2, μ = 1.297 mm^{-1}, $F(000)$ = 2704. Unit cell parameters were determined by nonlinear least-squares refinement of 54 reflections ($10 < 2\theta < 28°$). A total of 5597 reflections were collected in the range $4 < 2\theta < 50°$, crystal stability was monitored by recording 3 check reflections every 100 reflections, and data were corrected for a decay of 2.5%. Data were corrected for Lorentz and polarization effects, and an empirical absorption correction, based on ψ-scans, was applied (T_{max} = 0.737, T_{min} = 0.646). The structure was solved by direct methods (TREF[31]) and refined by full-matrix least-squares on F^2, using all 5212 independent reflections (R_{int} = 0.046). The refinement, on 392 parameters, converged with wR2 = 0.2494, goodness of fit = 1.124 (all data), and conventional R1 = 0.0965 (2σ data). The systematic absences fit $C2$, Cm, or $C2/m$ and the structure will solve in all three, but the refinement is only stable in the highest symmetry space group, $C2/m$. The cation has $2/m$ symmetry. An uncoordinated triflate is located on, and disordered about, the mirror plane. A further region of electron density, disordered about both a mirror and a 2-fold axis and lying between layers of cations, has been modeled as a disordered water molecule. The only significant residual electron density peaks are in this region or very close to the Eu ions. All the non-hydrogen atoms were refined with anisotropic atomic displacement parameters except for the disordered or partial occupancy solvate molecules. Hydrogen atoms were added at calculated positions for the cation only.

Both data sets were collected on a Siemens P4 diffractometer with graphite-monochromated Mo Kα radiation (λ = 0.710 73 Å) at 153(2) K. The structures were refined using the SHELXL-93 package.[32]

Preparation of Ligands. 6-(*N*,*N*-Diethylcarbamoyl)pyridine-2-carboxylic acid[24] (**1**) and 3,3′-dinitro-4,4′-bis(*N*-alkylamino)diphenylmethane (alkyl = methyl (**2**), ethyl (**3**))[33] were prepared according to literature procedures.

***N*,*N*′-Dialkyl-*N*,*N*′-[methylenebis(2-nitrophen-1,4-ylene]bis(6-(*N*,*N*-diethylcarbamoyl)pyridine-2-carboxamide) (Alkyl = Methyl (4), Ethyl (5)).** A 500 mg (2.25 mmol) amount of 6-(*N*,*N*-diethylcarbamoyl)pyridine-2-carboxylic acid (**1**), freshly distilled thionyl chloride (2.70 g, 22.3 mmol), and DMF (100 μL) were refluxed for 90 min in dry dichloromethane (60 mL) under an inert atmosphere. On evaporation and pumping for 1 h, a pale yellow solid was formed. This was redissolved in 50 mL of dry dichloromethane and added dropwise to a stirred solution of 3,3′-dinitro-4,4′-bis(*N*-alkylamino)diphenylmethane (alkyl = methyl (**2**), 355 mg, 1.13 mmol, and ethyl (**3**), 387 mg, 1.13 mmol) and triethylamine (430 mg, 4.25 mmol) in 30 mL of dichloromethane. The solution was refluxed under an inert atmosphere for 5 h and evaporated. The brown residue was partitioned between dichloromethane (2 × 100 mL) and half-saturated NH_4Cl (100 mL) solution. The combined organic phase was dried over Na_2SO_4 and evaporated, and the resulting crude solid was purified by column chromatography (silica gel; CH_2Cl_2/MeOH, 99.2:0.8 → 98:2) to give **4** (65% yield) and **5** (60% yield) (see Scheme 1). ^{1}H-NMR in $CDCl_3$: **4**, δ 0.8−1.2 (12H, m), 2.8−3.6 (14H, m), 4.2−4.6 (2H, m), 6.8−8.1 (12H, m); **5**, δ 0.8−1.2 (18H, m), 2.8−3.7 (12H, m), 4.2−4.5 (2H, m), 6.8−8.3 (12H, m).

Bis{1-alkyl-2-[6′-(*N*,*N*-diethylcarbamoyl)pyridin-2′-yl]benzimidazol-5-yl}methane (Alkyl = Methyl (L^5), Ethyl (L^6)). Freshly activated iron powder (1.11 g, 19.89 mmol) and HCl (37%, 4.97 mL, 50.0 mmol) were added to a solution of **4** (480 mg, 0.66 mmol) or **5** (496 mg, 0.66 mmol) in ethanol/water (132:33.8 mL). The mixture was refluxed overnight under an inert atmosphere. The golden colored solution was cooled, filtered, and evaporated to remove the ethanol. Water was added to bring the total volume to 100 mL before the pH was adjusted to 7 using aqueous NH_4OH (12%). The green blue gelatinous hydroxide which formed during this procedure turned to the orange oxide on addition of H_2O_2 solution (30%, 1 mL). The pH was then increased to 8.5 before 250 mL of dichloromethane was added. The two phases underwent vigorous agitation with slight warming before separation. This extraction procedure was repeated twice more, and the organic phases were combined, dried over Na_2SO_4, filtered, and evaporated to dryness, resulting in a pale brown crude solid which was purified by column chromatography (silica gel; CH_2Cl_2/MeOH, 98.5:1.5 → 97:3) and then crystallized from hot MeCN to give a colorless crystalline solid in relatively high yield (L^5, 68%; L^6, 57%).

(28) Gampp, H.; Maeder, M.; Meyer, C. J.; Zuberbühler, A. D. *Talanta* **1986**, *33*, 943−951.
(29) Hopfgartner, G.; Piguet, C.; Henion, J. D.; Williams, A. F. *Helv. Chim. Acta* **1993**, *76*, 1759−1766.
(30) Hopfgartner, G.; Piguet, C.; Henion, J. D. *J. Am. Soc. Mass Spectrom.* **1994**, *5*, 748−756.
(31) Sheldrick, G. M. *Acta Crystallogr., Sect A* **1990**, *46*, 467−473.
(32) Sheldrick, G. M. SHELXL-93, University of Göttingen.
(33) Piguet, C.; Bernardinelli, G.; Bocquet, B.; Quattropani, A.; Williams, A. F. *J. Am. Chem. Soc.* **1992**, *114*, 7440−7451.

Scheme 1

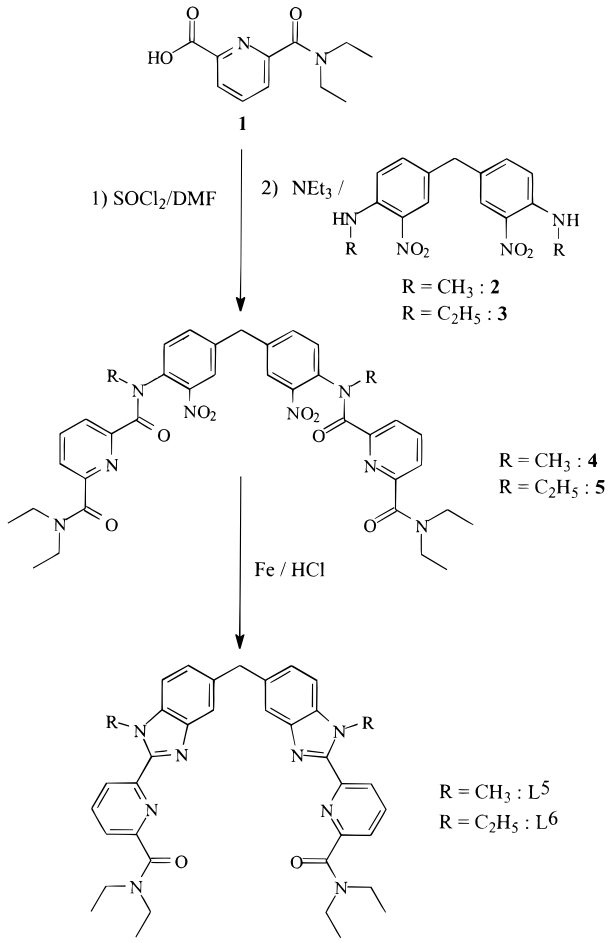

L[5]. Anal. Calcd for $C_{37}H_{40}N_8O_2 \cdot H_2O$: C, 68.65; H, 6.49; N, 17.32. Found: C, 68.48; H, 6.51; N, 17.24. ^{1}H-NMR in CD_3CN: δ 8.32 (2H, d, $J^3 = 8$ Hz), 8.15 (2H, t, $J^3 = 8$ Hz), 7.67 (2H, s), 7.49 (2H, d, $J^3 = 8$ Hz), 7.34 (2H, d, $J^3 = 8$ Hz), 7.14 (2H, d, $J^3 = 8$ Hz), 4.23 (6H, s), 4.11 (2H, s), 3.34 (4H, q, $J^3 = 7.2$ Hz), 3.58 (4H, q, $J^3 = 7.2$ Hz), 1.21 (6H, t, $J^3 = 7.2$ Hz), 1.06 (6H, t, $J^3 = 7.2$ Hz).

L[6]. Anal. Calcd for $C_{39}H_{44}N_8O_2 \cdot H_2O$: C, 69.35; H, 6.82; N, 16.59. Found: C, 69.30; H, 6.88; N, 16.59. ^{1}H-NMR in CD_3CN: δ 8.35 (2H, d, $J^3 = 8$ Hz), 8.01 (2H, t, $J^3 = 8$ Hz), 7.65 (2H, s), 7.52 (2H, d, $J^3 = 8$ Hz), 7.50 (2H, d, $J^3 = 8$ Hz), 7.27 (2H, d, d, $J^3 = 8$, $J^4 = 12$ Hz), 4.76 (4H, q, $J^3 = 7.2$ Hz), 4.21 (2H, s), 3.55 (4H, q, $J^3 = 7.2$ Hz), 3.34 (4H, q, $J^3 = 7.2$ Hz), 1.40 (6H, t, $J^3 = 7.2$ Hz), 1.22 (6H, t, $J^3 = 7.2$ Hz), 1.05 (6H, t, $J^3 = 7.2$ Hz).

Preparation of the Complexes. The perchlorate salts $Ln(ClO_4)_3 \cdot nH_2O$ (Ln = La, Nd, Eu, Gd, Tb, Ho, Lu; $n = 6-8$) were prepared from the corresponding oxides (Rhône-Poulenc, 99.99%) according to the literature method.[34] ***Caution!*** *Perchlorate salts combined with organic ligands are potentially explosive and should be handled with the necessary precautions.*[35]

Preparation of $[Ln_2(L^5)_3](ClO_4)_6 \cdot nH_2O$ (Ln = La (6), Eu (7)). A 51.5 μmol amount of $Ln(ClO_4)_3 \cdot nH_2O$ in acetonitrile (5 mL) was slowly added to a solution of L^5 (50 mg, 77 μmol) in dichloromethane (5 mL). After being stirred at room temperature for 1 h, the solution was evaporated, the solid residue was re-dissolved in 1:1 acetonitrile/propionitrile, the solution was filtered, and tetrahydrofuran was diffused into the solution for 3−4 days. The colorless cube-shaped crystals were isolated by filtration in 78−81% yield and dried under high vacuum at 60 °C for 24 h. The number of solvent molecules depends greatly on the drying conditions used during the synthesis and must be determined for each individual batch.

Preparation of Eu-Doped $[Ln_2(L^5)_3](ClO_4)_6 \cdot nH_2O$, (Ln = La (7a), Gd (7b)). Eu-doped (2%) complexes were isolated for the purpose of determining if structural changes occur in the series La−Gd. They were prepared as above using a mixed Ln/Eu solution (98:2).

Preparation of $[Ln_2(L^6)_3](ClO_4)_6 \cdot nH_2O$ (Ln = La (8), Eu (9), Gd (10), Tb (11), Lu (12)). A solution of $Ln(ClO_4)_3 \cdot nH_2O$ (49.4 μmol) in acetonitrile (5 mL) was slowly added to a solution of L^5 (50 mg, 74 μmol) in dichloromethane (5 mL). After being stirred at room temperature for 1 h, the solution was evaporated, the solid residue was redissolved in 1:1 acetonitrile/propionitrile, the solution was filtered, and tetrahydrofuran was diffused into the solution for 3−4 days. The resulting white microcrystalline aggregates were collected by filtration and dried to give complexes $[Ln_2(L^6)_3](ClO_4)_6 \cdot nH_2O$ (Ln = La (n = 7), Eu (n = 5), Gd (n = 7), Tb (n = 1), Lu (n = 4)) in 81−89% yields. In the case of complex **11** a number of crystals of X-ray quality were also isolated.

Preparation of $[Eu_2(L^6)_2](CF_3SO_3)_6 \cdot 7H_2O$ (13). $Eu(CF_3SO_3)_3 \cdot 3.4H_2O$ (33 mg, 49 μmol) was dissolved in acetonitrile (3 mL), and the solution was added dropwise, with stirring, to a solution of L^6 (50 mg, 74 μmol) dissolved in CH_2Cl_2 (3 mL). After 1 h of agitation at room temperature, the solution was evaporated to dryness producing **13** as a white solid which was redissolved in approximately 3 mL of acetonitrile and filtered. Fragile colorless single crystals of $[Eu_2(L^6)_2(CF_3SO_3)_4(H_2O)_2](CF_3SO_3)_2(MeOH)_2(H_2O)_{5.5}$ (**13a**) were obtained by slow diffusion of diethyl ether into a concentrated acetonitrile solution.

Each of the complexes **6**−**13** gave satisfactory elemental analyses and IR spectra (Tables S1 and S2 in the Supporting Information).

Results

Preparation of Ligands and Complexes. Bis{1-alkyl-2-[6′-(*N*,*N*-diethylcarbamoyl)pyridin-2′-yl]benzimidazol-5-yl}-methane (alkyl = methyl (L^5), ethyl (L^6)) were obtained in good yields according to a previously described two-step procedure involving a modified Phillips type coupling reaction as the key step in achieving the desired benzimidazole units from *N*-(2-nitroaryl)arenecarboxamide precursors.[36] Reaction of $L^{5,6}$ with stoichiometric amounts of $Ln(ClO_4)_3 \cdot nH_2O$ (Ln = La, Eu, Gd, Tb, Lu) in acetonitrile gives colorless solutions from which the complexes $[Ln_2(L^5)_3](ClO_4)_6 \cdot nH_2O$ (Ln = La (**6**), Eu (**7**)) and $[Ln_2(L^6)_3](ClO_4)_6 \cdot nH_2O$ (Ln = La (**8**), Eu (**9**), Gd (**10**), Tb (**11**), Lu (**12**)) can be crystallized in 78−89% yield. The complexes display a number of identifying IR bands including (i) the characteristic ligand vibrational peaks in the range 1600−600 cm^{-1},[26] (ii) an intense carbonyl stretching vibration which is red shifted to ca 1590 cm^{-1} with respect to the free ligand (1631 cm^{-1}),[37] (iii) uncoordinated H_2O molecules at 3400 and 1620 cm^{-1}, and (iv) typical vibrations from ionic ClO_4^- anions at 1095 and 625 cm^{-1}.[38] Attempts to prepare similar 2:3 complexes from L^6 and $Eu(CF_3SO_3)_3 \cdot 3.4H_2O$ failed, and the 2:2 complex $[Eu_2(L^6)_2](CF_3SO_3)_6 \cdot 7H_2O$ (**13**) has been isolated. Its IR spectrum in the fingerprint region shows bands associated with the ligand together with a broad and largely split band appearing at ca 1263 cm^{-1}, associated with the coexistence of ionic and coordinated triflate anions.[37]

Crystal Structure of $[Tb_2(L^6)_3](ClO_4)_6(THF)_{0.5}(MeCN)_2(EtOH)_{0.5}$ (11a). Fragile colorless cube-shaped single crystals were isolated after slow diffusion of diethyl ether into a concentrated acetonitrile/propionitrile (1:1) solution of **11**.

(34) Desreux, J. F. In *Lanthanide Probes in Life, Chemical and Earth Sciences*; Bünzli, J.-C. G., Choppin, G. R., Eds.; Elsevier Publishing Co.: Amsterdam, 1989; Chapter 2, p 43.
(35) Wolsey, W. C. *J. Chem. Educ.* **1978**, *55*, A355.
(36) Piguet, C.; Bocquet, B.; Hopfgartner, G. *Helv. Chim. Acta* **1994**, *77*, 931−942.
(37) Renaud, F.; Piguet, C.; Bernardinelli, G.; Bünzli, J.-C. G.; Hopfgartner, G. *Chem. Eur. J.* **1997**, *3*, 1646−1659; 1660−1667.
(38) Nakamoto, K. *Infrared and Raman Spectra of Inorganic and Coordination Compounds*, 3rd ed.; J. Wiley: New York, Chichester, Brisbane, and Toronto, 1972; pp 142−154.

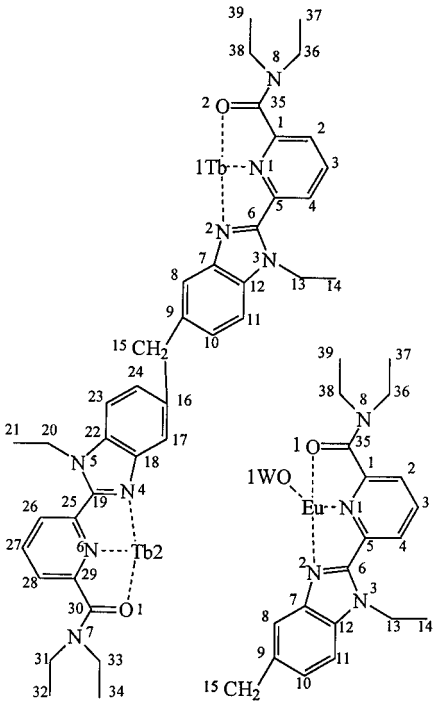

Figure 1. Atom-numbering scheme for $[Tb_2(L^6)_3]^{6+}$ in **11a** and $[Eu_2(L^6)_2(CF_3SO_3)_4(H_2O)_2]^{2+}$ in **13a**.

However when isolated from the mother liquor, the crystals quickly disintegrate into a microcrystalline powder which displays elemental analyses and IR spectrum compatible with the replacement of the volatile organic solvent molecules with H_2O. The atom-numbering scheme for **11a** is given in Figure 1, and an ORTEP[39] stereoscopic view of the cationic helicate $[Tb_2(L^6)_3]^{6+}$ is displayed on Figure 2. Selected bond lengths and angles are reported in Table 1, while atomic coordinates and other relevant information are given in the Supporting Information (Tables S3.1−S3.5; Figures F1, F2). The structure features dinuclear helical and pseudotrigonal cations. Each cation contains two Tb ions and three wrapped ligand strands composing a triple helical structure with no crystallographically imposed symmetry. Each ligand strand is coordinated to Tb(1) via the carbonyl oxygen, pyridine, and benzimidazole nitrogen atoms at one end of the strand, and the second terbium (Tb(2)) is coordinated by the related donor set from the other end of the ligand. Consequently, the Tb ions are nine-coordinate and are separated by 9.06(3) Å, a distance comparable to that found in the analogous complex $[Eu_2(L^4)_3]^{6+}$ (8.876(3) Å).[26] A detailed structural analysis shows that the two Tb atoms are located in very similar pseudo-tricapped trigonal prismatic coordination sites. The Tb−O and Tb−N distances do not deviate significantly from their average values (2.36 and 2.58 Å, respectively). The effective ionic radii of Tb(III) calculated using Shannon's definition with $R(O) = 1.31$ Å and $R(N) = 1.46$ Å amount to 1.086 Å (Tb(1)) and 1.104 Å (Tb(2)) in good agreement with the reported value for nine-coordinate Tb(III) complexes (1.095 Å).[40] A close scrutiny of the benzimidazole rings reveals that they do not meet the criteria generally accepted for $\pi-\pi$ stacking interactions, that is, a parallel overlap of the aromatic rings separated by approximately 3.4 Å.[41] In **11a** the mean plane of the benzimidazole group containing N(2c) and N(3c) is almost parallel (12°) to that containing N(4a) and N(5a)

Table 1. Selected Bond Lengths (Å) and Bond Angles (deg) for $[Tb_2(L^6)_3](ClO_4)_6(THF)_{0.5}(MeCN)_2(EtOH)_{0.5}$ (**11a**)

Distances			
Tb(1)−O(2A)	2.330(5)	Tb(2)−O(1A)	2.396(6)
Tb(1)−O(2B)	2.407(5)	Tb(2)−O(1B)	2.362(6)
Tb(1)−O(2C)	2.354(5)	Tb(2)−O(1C)	2.336(6)
Tb(1)−N(1A)	2.588(6)	Tb(2)−N(6A)	2.576(6)
Tb(1)−N(1B)	2.528(6)	Tb(2)−N(6B)	2.574(7)
Tb(1)−N(1C)	2.586(7)	Tb(2)−N(6C)	2.620(6)
Tb(1)−N(2A)	2.544(6)	Tb(2)−N(4A)	2.653(6)
Tb(1)−N(2B)	2.573(7)	Tb(2)−N(4B)	2.564(7)
Tb(1)−N(2C)	2.558(6)	Tb(2)−N(4C)	2.543(7)

Angles			
O(2A)−Tb(1)−O(2C)	80.8(2)	O(1C)−Tb(2)−O(1B)	82.2(2)
O(2A)−Tb(1)−O(2B)	79.4(2)	O(1C)−Tb(2)−O(1A)	82.4(2)
O(2C)−Tb(1)−O(2B)	77.8(2)	O(1B)−Tb(2)−O(1A)	79.6(2)
O(2A)−Tb(1)−N(1B)	67.4(2)	O(1C)−Tb(2)−N(4C)	124.9(2)
O(2C)−Tb(1)−N(1B)	132.7(2)	O(1B)−Tb(2)−N(4C)	142.0(2)
O(2B)−Tb(1)−N(1B)	62.9(2)	O(1A)−Tb(2)−N(4C)	78.7(2)
O(2A)−Tb(1)−N(2A)	126.1(2)	O(1C)−Tb(2)−N(4B)	82.8(2)
O(2C)−Tb(1)−N(2A)	83.2(2)	O(1B)−Tb(2)−N(4B)	126.9(2)
O(2B)−Tb(1)−N(2A)	145.2(2)	O(1A)−Tb(2)−N(4B)	147.1(2)
N(1B)−Tb(1)−N(2A)	143.9(2)	N(4C)−Tb(2)−N(4B)	86.1(2)
O(2A)−Tb(1)−N(2C)	139.4(2)	O(1C)−Tb(2)−N(6B)	66.3(2)
O(2C)−Tb(1)−N(2C)	127.1(2)	O(1B)−Tb(2)−N(6B)	62.9(2)
O(2B)−Tb(1)−N(2C)	79.4(2)	O(1A)−Tb(2)−N(6B)	133.1(2)
N(1B)−Tb(1)−N(2C)	72.1(2)	N(4C)−Tb(2)−N(6B)	148.0(2)
N(2A)−Tb(1)−N(2C)	89.6(2)	N(4B)−Tb(2)−N(6B)	64.5(2)
O(2A)−Tb(1)−N(2B)	79.4(2)	O(1C)−Tb(2)−N(6A)	135.7(2)
O(2C)−Tb(1)−N(2B)	143.4(2)	N(4B)−Tb(2)−N(6B)	64.5(2)
O(2B)−Tb(1)−N(2B)	127.6(2)	O(1A)−Tb(2)−N(6A)	63.8(2)
N(1B)−Tb(1)−N(2B)	64.7(2)	N(4C)−Tb(2)−N(6A)	77.4(2)
N(2A)−Tb(1)−N(2B)	84.0(2)	N(4B)−Tb(2)−N(6A)	140.6(2)
N(2C)−Tb(1)−N(2B)	86.8(2)	N(6B)−Tb(2)−N(6A)	117.0(2)
O(2A)−Tb(1)−N(1C)	136.0(2)	O(1C)−Tb(2)−N(6C)	62.5(2)
O(2C)−Tb(1)−N(1C)	64.4(2)	O(1B)−Tb(2)−N(6C)	134.6(2)
O(2B)−Tb(1)−N(1C)	68.1(2)	O(1A)−Tb(2)−N(6C)	68.9(2)
N(1B)−Tb(1)−N(1C)	117.7(2)	N(4C)−Tb(2)−N(6C)	62.4(2)
N(2A)−Tb(1)−N(1C)	77.4(2)	N(4B)−Tb(2)−N(6C)	78.2(2)
N(2C)−Tb(1)−N(1C)	62.9(2)	N(6B)−Tb(2)−N(6C)	119.0(2)
N(2B)−Tb(1)−N(1C)	144.2(2)	N(6A)−Tb(2)−N(6C)	122.3(2)
O(2A)−Tb(1)−N(1A)	63.0(2)	O(1C)−Tb(2)−N(4A)	141.0(2)
O(2C)−Tb(1)−N(1A)	68.0(2)	O(1B)−Tb(2)−N(4A)	79.5(2)
O(2B)−Tb(1)−N(1A)	132.0(2)	O(1A)−Tb(2)−N(4A)	126.9(2)
N(1B)−Tb(1)−N(1A)	120.5(2)	N(4C)−Tb(2)−N(4A)	89.2(2)
N(2A)−Tb(1)−N(1A)	63.2(2)	N(4B)−Tb(2)−N(4A)	81.3(2)
N(2C)−Tb(1)−N(1A)	148.6(2)	N(6B)−Tb(2)−N(4A)	74.7(2)
N(2B)−Tb(1)−N(1A)	75.5(2)	N(6A)−Tb(2)−N(4A)	63.1(2)
N(1C)−Tb(1)−N(1A)	120.5(2)	N(6C)−Tb(2)−N(4A)	145.8(2)

but the shortest distance from an atom in one ring to the mean plane of the other is 3.9 Å. Similarly, the mean plane of the benzimidazole group containing N(4c) and N(5c) and that of the ring containing N(2b) and N(3b) are separated by a mean distance of 3.9 Å and tilted at 22°. The conclusion is that $\pi-\pi$ interactions are weak and unlikely to be significant in determining the conformation of the cation as similarly reported for $[Eu_2(L^4)_3]^{6+}$.[26]

Crystal Structure of $[Eu_2(L^6)_2(CF_3SO_3)_4(H_2O)_2](CF_3SO_3)_2(MeOH)_2(H_2O)_{5.5}$ (13a). Selected bond lengths and angles are given in Table 2. Figure 1 shows the atom-numbering scheme, and Figure 3 displays an ORTEP[39] stereoview of the $[Eu_2(L^6)_2(CF_3SO_3)_4(H_2O)_2]^{2+}$ cation. Atomic coordinates and other relevant data are reported in the Supporting Information (Tables S4.1−S4.5; Figures F3, F4). The cation has 2/*m* symmetry, the Eu ions sit on a 2-fold axis, and a mirror plane bisects the Eu−Eu vector, passing through C(15) and its symmetry equivalents. The Eu ions are 9-coordinate, bonded to the

(39) Johnson C. K., *ORTEP II*; Report ORNL-5138; Oak Ridge National Laboratory: Oak Ridge, TN, 1976.
(40) Shannon, R. D. *Acta Crystallogr*. **1976**, *A32*, 751−767.
(41) Hunter C. A.; Sanders J. K. M. *J. Am. Chem. Soc*. **1990**, *112*, 5525−5534. Adams, H.; Carver, F. J.; Hunter, C. A.; Morales, J. C.; Seward, E. M. *Angew Chem., Int. Ed. Engl.* **1996**, *35*, 1542−1544.

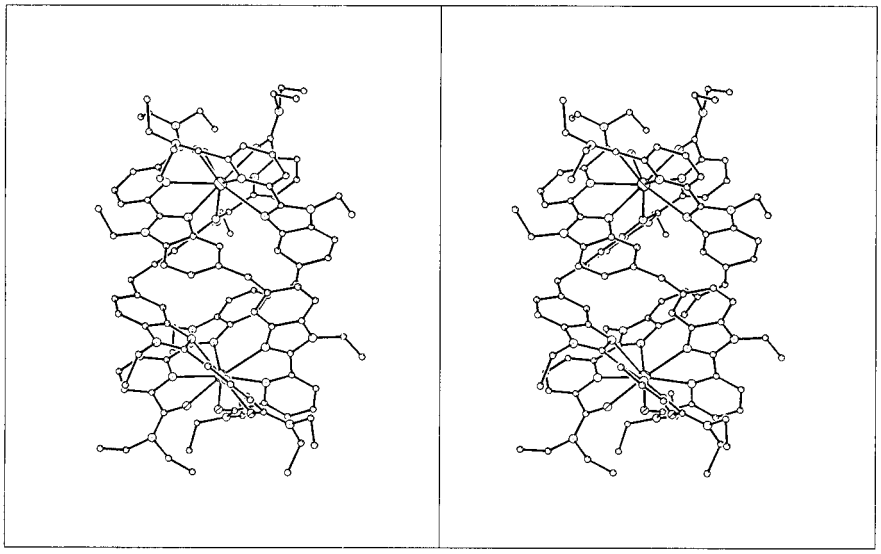

Figure 2. ORTEP stereoview of the $[Tb_2(L^6)_3]^{6+}$ cation perpendicular to the pseudo-C_3 axis in (**11a**).

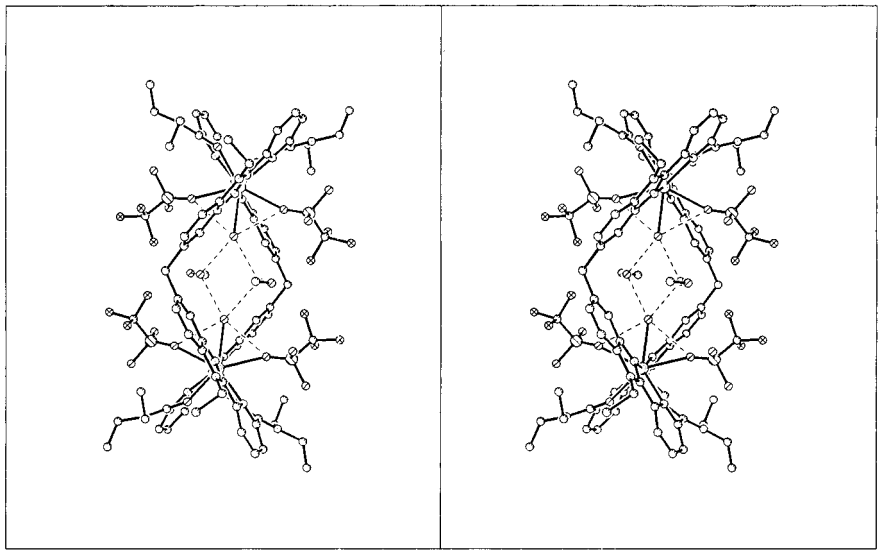

Figure 3. ORTEP stereoview of the $[Eu_2(L^6)_2(CF_3SO_3)_4(H_2O)_2]^{2+}$ cation in **13a**, perpendicular to the C_2 axis.

Table 2. Selected Bond Lengths (Å) and Bond Angles (deg) for $[Eu_2(L^6)_2(CF_3SO_3)_4(H_2O)_2](CF_3SO_3)_2(MeOH)_2(H_2O)_{5.5}$ (**13a**)[a]

Distances			
Eu-O(1)	2.409(8)	Eu-N(2)	2.547(9)
Eu-O(31)	2.451(8)	Eu-N(1)	2.615(10)
Eu-O(1W)	2.458(11)		
Angles			
O(1)*-Eu-O(1)	85.8(4)	O(1)*-Eu-O(31)	139.9(3)
O(1)-Eu-O(31)	75.4(3)	O(31)*-Eu-O(31)	139.0(4)
O(1)-Eu-O(1W)	137.1(2)	O(31)-Eu-O(1W)	69.5(2)
O(1)-Eu-N(2)*	71.9(3)	O(31)-Eu-N(2)*	81.7(3)
O(1)-Eu-N(2)	125.8(3)	O(31)-Eu-N(2)	90.8(3)
O(1W)-Eu-N(2)	79.2(2)	N(2)*-Eu-N(2)	158.5(4)
O(1)-Eu-N(1)*	67.4(3)	O(31)-Eu-N(1)*	134.3(3)
N(2)-Eu-N(1)*	132.5(3)	O(1)-Eu-N(1)	63.4(3)
O(31)*-Eu-N(1)	134.3(3)	O(31)-Eu-N(1)	72.5(3)
O(1W)-Eu-N(1)	124.6(2)	N(2)-Eu-N(1)	62.4(3)
N(1)*-Eu-N(1)	110.8(5)		

[a] Symmetry transformations used to generate equivalent atoms: * = $-x, y, -z$.

pyridine, benzimidazole, and carbonyl groups of two ligand molecules as well as to two triflate ions and one water molecule (Eu−Eu = 9.05(3) Å). The coordination sphere may be loosely described as a distorted monocapped square antiprism flattened along the pseudo-C_4 axis. O(1), N(1), O(1)*, N(1)* and O(31), N(2), O(31)*, N(2)* form the two facial planes while the oxygen atom of the bound water molecule occupies the capping position. The Eu−O(amide) and Eu−N(benzimidazole) bond distances are standard,[17,18,24,26] while the Eu−N(pyridine) bond is longer as a result of a significant tilt of the pyridine ring (Eu lies 0.38 Å out of the plane of the pyridine ring, Figure 3), which leads to a bent conformation of the tridentate units as previously observed in $[EuZn(L^3)_3]^{5+}$.[24] Each ligand is coordinated to two Eu atoms located on the same side of the strand thus producing an unsaturated side-by-side double-stranded helicate with zero net helicity[16] which strongly contrasts with the triple helical arrangement found in $[Tb_2(L^6)_3]^{6+}$. The two Eu(III) ions are connected through four hydrogen-bonded water molecules (O(1w)−O(2w) = 2.78(2) Å). The four coordinated triflate anions are also involved in hydrogen bonding (Figure 3, O(1w)−O(31) = 2.80 Å).

Photophysical Properties of Crystalline Complexes 9−13. Under excitation at 31 153 cm^{-1} (77 K) L^5 and L^6 present very similar emission spectra in which two broad bands were observed (Table 3; excitation spectra are reported in Figure F6,

Table 3. Ligand-Centered Absorption and Emission Properties

compd	$\pi \rightarrow \pi^*$[a]	$\pi \rightarrow \pi^*$[b]	$^1\pi\pi^*$[c]	$^3\pi\pi^*$[c]	$\tau(^3\pi\pi^*)$[c]
L^6	31 200 (45 820) 41 322 (broad sh) 43 670 (43 660)	31 008 40 650 (sh)	24 331	21 277 (sh) 20 040 18 939 (sh)	4.2 ± 0.2
$[Eu_2(L^6)_3]^{6+}$ (**9**)	29 762 (90 500) 40 650 (66 640) 48 876 (212 797)	42 735 (sh) 30 864 29 850 (sh)	23 890	*d*	*d*
$[Gd_2(L^6)_3]^{6+}$ (**10**)	29 325 (90 470) 40 322 (65 900) 49 687 (212 340)		27 473 (sh) 25 445 24 272 22 988 (sh) 21 739 (sh) 20 747 (sh)	20 934 19 697 18 453	14 ± 2
$[Tb_2(L^6)_3]^{6+}$ (**11**)	29 498 (90 900) 40 322 (66 750) 48 832 (213 737)	42 373 (sh) 29 154	23 890	*d*	*d*
$[Lu_2(L^6)_3]^{6+}$ (**12**)	29 691 (90 600) 40 485 (66 640) 48 734 (213 032)		22 935	20 202 (sh) 19 011 17 953 (sh)	90 ± 5

[a] Electronic spectral data in acetonitrile at 295 K; energies are given for the maximum of the band envelope in cm^{-1}, and ϵ (within parenthesis), in $M^{-1}\cdot cm^{-1}$; sh = shoulder. [b] Reflectance spectra recorded at 295 K (see Figure F5, Supporting Information). [c] Luminescence data and lifetimes (ms) at 77 K. [d] $^3\pi\pi^*$ luminescence quenched by transfer to the Ln ion.

Supporting Information). The first band with a maximum at 24 330 cm^{-1} quickly diminishes in intensity when a short time delay (0.1 ms) is enforced and therefore has been attributed to the $^1\pi\pi^*$ state. The second band displays a maximum at approximately 20 040 cm^{-1} and is more structured with a number of weak low- and high-energy shoulders, representing a vibrational progression of about 1200 cm^{-1} attributable to a ring-breathing mode (1450 cm^{-1} in the fundamental state). This band has a single-exponential time decay with a lifetime of 4.2 $\pm$ 0.2 ms and is therefore assigned to the $^3\pi\pi^*$ state. Upon complexation of Gd(III) and Lu(III), both the ligand-based singlet and triplet state emission bands were observed to shift in a progressive manner to lower energies as a consequence of the greater charge density exhibited by the Lu(III) ion over the Gd(III) ion resulting in a stronger bond particularly with the C═O group. Extensive vibrational fine structure is observed for both singlet (ca. 1170 cm^{-1}) and triplet (1240 cm^{-1}) states in the Gd compound. A significant increase in the lifetime (from 4.2 to 90 ms) of the triplet state was recorded upon complexation to Lu(III). In complete contrast the emission from the $^3\pi\pi^*$ state upon excitation through the $^1\pi\pi^*$ transition of the $[Eu_2(L^5)_3]^{6+}$ (**7**), $[Tb_2(L^6)_3]^{6+}$ (**11**), and $[Eu_2(L^6)_2(CF_3SO_3)_4(H_2O)_2]^{2+}$ (**13**) complexes is completely quenched and the characteristic bands of the Eu and Tb ions are clearly evident as depicted in Figure 4. Typically, nonradiative deexcitation of the Eu($^5D_1$) and Eu($^5D_2$) states prevents observation of the associated transitions to ^7F_J, but the observation of emission bands at 18 416 cm^{-1} ($^5D_1 \rightarrow {}^7F_1$), 17 825 cm^{-1} ($^5D_1 \rightarrow {}^7F_2$), and 21 740 cm^{-1} ($^5D_2 \rightarrow {}^7F_0$) at 77 K in the spectra of the $[Eu_2(L^i)_3]^{6+}$ (i = 5, 6) cations points to a sizable energy transfer process between the triplet state of the ligand (0-phonon transition at $\approx$20 900 cm^{-1} in $[Gd_2(L^5)_3]^{6+}$) and the Eu($^5D_{1,2}$) states for the Eu complexes of L^5 and L^6.[1]

Since both the Eu and Tb complexes of L^5 are strongly luminescent, we have examined further their properties in the solid state at 295, 77, and 10 K for the purpose of investigating the coordination environment around the luminescent ion and analyzing the energy migration pathways. The excitation spectrum of $[Eu_2(L^5)_3]^{6+}$ (**7**) at 77 K produces a broad and intense band with a maximum at 24 746 cm^{-1}, corresponding to excitation through the $^1\pi\pi^*$ ligand state. The emission spectrum obtained upon excitation though the $^1\pi\pi^*$ level at the same temperature is well resolved but typical of a compound

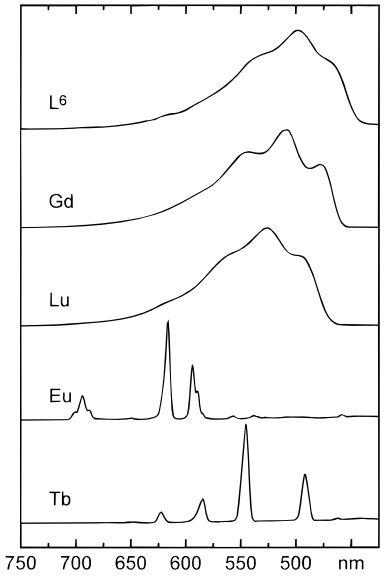

Figure 4. Phosphorescence emission spectra of L^6 and complexes **9**−**11** measured at 77 K.

with at least two different Eu(III) sites; viz., the $^5D_0 \rightarrow {}^7F_1$ transition clearly displays four components (Figure 5). Typically, a narrow symmetrical $^5D_0 \rightarrow {}^7F_0$ band arises from an emitting species containing a single Eu(III) coordination environment; however for complex **7** this very weak band (1% of the intensity of the magnetic dipole $^5D_0 \rightarrow {}^7F_1$ transition (see Table S5, Supporting Information) was found to be split at 77 K into two broad components (full width at half-height, fwhh, ca. 17 cm^{-1}) with two distinct maxima at 17 216 cm^{-1} (580.8 nm, site I) and 17 235 cm^{-1} (580.2 nm, site II). Excitation spectra recorded with the analyzing wavelength set on components of either the $^5D_0 \rightarrow {}^7F_1$ or the $^5D_0 \rightarrow {}^7F_2$ transition revealed additional constituents. In fact when the excitation wavelength is scanned through the 0−0 band profile, different emission spectra with similar overall band shape and relative intensities but distinct fine splittings were recorded (see Figure 5), indicating that site I reflects at least two somewhat different chemical environments for Eu(III), sites Ia and Ib. The crystal field splittings of the spectra can be interpreted in terms of a pseudotrigonal symmetry, derived from the crystallographic study of **11a**, as follows:[1,26] The extremely weak $^5D_0 \rightarrow {}^7F_0$

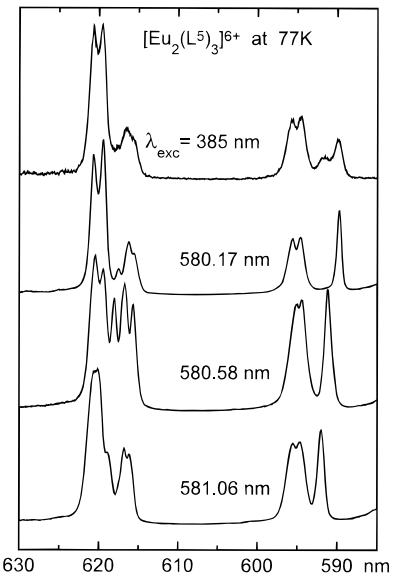

Figure 5. Emission spectra of $[Eu_2(L^5)_3]^{6+}$ at 77 K measured under various excitation conditions.

Table 4. Lifetimes of the Eu($^5D_0$) and Tb($^5D_4$) Excited Levels (ms) in $[Ln_2(L^i)_3]^{6+}$ (Ln = Eu, Tb, i = 5, 6; Ln = Eu-Doped La, Gd, i = 5) under Various Excitation Conditions

compd	T (K)	λ_{exc} (nm)	τ (ms)
$[Eu_2(L^4)_3]^{6+}$ [a]	250	580.5	0.63 ± 0.07
	77		2.03 ± 0.04
$[Eu_2(L^5)_3]^{6+}$ (**7**)	295	580.2	2.11 ± 0.05
site II	77	580.17	2.01 ± 0.13
site Ib		580.67	2.36 ± 0.10
site Ia		581.06	2.66 ± 0.17
$[La_2(L^5)_3]^{6+}$−2% Eu (**7a**)	295	308	2.16 ± 0.22
	77		2.28 ± 0.14
$[Gd_2(L^5)_3]^{6+}$−2% Eu (**7b**)	295		1.95 ± 0.15
	77		2.25 ± 0.16
$[Eu_2(L^6)_3]^{6+}$ (**9**)	77	580.5	2.09 ± 0.21
		308	2.44 ± 0.09
	10	580.5	2.28 ± 0.27
		308	2.42 ± 0.11
$[Eu_2(L^6)_2]^{6+}$ (**13**)	295	579.5	0.68 ± 0.02
	77	580.8	0.76 ± 0.02
	10		0.77 ± 0.02
$[Tb_2(L^6)_3]^{6+}$ (**11**)	295	308	0.061 ± 0.003
	77	308	1.96 ± 0.04
		488	1.81 ± 0.06

[a] Acetonitrile solvate; data from ref 26.

transition is consistent with the fact that it is symmetry forbidden in the D_3 group. The $^5D_0 \rightarrow {}^7F_1$ transition is split into one singlet and one closely spaced doublet where the singlet can be assigned to the $A_1 \rightarrow A_2$ and the doublet to the $A_1 \rightarrow E$ transition; the more complicated $^5D_0 \rightarrow {}^7F_2$ transition displays a sharp five-line pattern consisting of two doublets assigned to the two allowed $A_1 \rightarrow E$ transitions in D_3 and a less intense singlet which is also derived from the $A_1 \rightarrow E$ crystal field splitting. Analysis of the $^5D_0 \rightarrow {}^7F_4$ transition shows six components, also consistent with a distorted trigonal symmetry.

The lifetimes recorded at 77 K at excitation wavelengths corresponding to the emission spectra reported in Figure 5 are longer than 2 ms (Table 4) and preclude the presence of 1 H_2O molecule in the inner coordination sphere. The Eu($^5D_0$) lifetime is almost temperature-independent, but it varies with the excitation wavelength, from 2.1 to 2.7 ms at 77 K. Therefore, both this variation and the crystal field splitting changes point to second-sphere effects arising from the interaction of solvent molecules with the ligand strands via H bonding,[42] thus

Table 5. Identified Eu(^7F_J) Crystal Field Levels (cm^{-1}, J = 1−4) in $[Eu_2(L^i)_3]^{6+}$ (i = 5, **7**; i = 6, **9**) from Luminescence Spectra at 77 K

	compd (λ_{exc}/cm^{-1})				
	7 (site II) (17 2367)	**7** (site Ib) (17 2247)	**7** (site Ia) (17 2109)	**9** (17 239)	$[Eu_2(L^4)_3]^{6+}$ [a] (17 2277)
$^7F_1$	280	309	318	277	295
	419	402	394	393	413
	446	421	419	422	431
$^7F_2$	991	982	980	998	
	1009	1010	998	1065	1000
	1043	1044	1052	1132	1029
	1093	1081	1084	1147	1086
	1125	1107	1099		1096
$^7F_3$	1829	1829	1827	*b*	1819
	1874	1876	1878		1871
	1893		1932		
	1924	1921			
	1942				
$^7F_4$	2720	2683	2688	2692	2707
	2736	2739	2713	2726	2720
	2804	2841	2810		2757
	2874	2878	2838	2864	2766
	2897	2986	2992	2998	2780
	3005	3012			2988

[a] From ref 26. [b] Too weak to be identified.

distorting the general coordination sphere of the Eu(III) ion. Indeed, we have shown recently that introduction of H_2O molecules in the lattice of $[Eu_2(L^4)_3]^{6+}$ results in a lowering of the symmetry, evident from the modification of the $^7F_1$ splitting.[26] From the spectra depicted in Figure 5, the two components of the transition to the $^7F_1$(E) level (using labels for trigonal symmetry) were calculated to be 27 (site II), 19 (site Ib), and 25 cm^{-1} (site Ia) apart while the total crystal field splitting of the $^7F_1$ level was respectively 166, 112, and 101 cm^{-1} (Table 5). The corresponding values reported for the crystals of $[Eu_2(L^4)_3]^{6+}$ grown in acetonitrile were 18 and 136 cm^{-1}, while 41 and 129 cm^{-1} were found for the same compound in which water was introduced into the lattice.[26] A qualitative population analysis of the $^5D_0 \rightarrow {}^7F_1$ transition[1] recorded under broad band excitation (Figure 5, top) reveals that site II is the more populated (ca. 70%). Since the elemental analysis of **7** was consistent with a single water molecule as the only solvent present for this compound (see Table S2, Supporting Information), we tentatively assign site II to the solvated $[Eu_2(L^5)_3]^{6+}$ cation. This would be consistent with the shorter lifetime of the $^5D_0$ level mostly attributable to quenching by the water molecule in the outer coordination sphere. The excitation spectrum of site II recorded at 77 K upon monitoring the high-energy $^5D_0 \rightarrow {}^7F_1$(A) component displays one relatively sharp band (fwhh = 10 cm^{-1}) at 17 238 cm^{-1} indicating a well-defined species. The other minor species evidenced in Figure 5 would then correspond to unsolvated species having a longer Eu($^5D_0$) lifetime and slightly different metal-ion environments, as often observed for microcrystalline materials.[43] We also note that in $[Tb_2(L^6)_3]^{6+}$ the two Tb(III) ions have slightly different mean Tb−N distances (2.56 ± 0.01 Å for Tb(1) and 2.59 ± 0.01 Å for Tb(2)). If such a difference exists for the Eu helicate, it could explain the occurrence of two slightly different Eu surroundings (sites Ia and Ib).

(42) Parker D.; Williams J. A. G. *J. Chem. Soc., Perkin Trans. 2* **1995**, 1305−1314.
(43) Nicolò, F.; Plancherel, D.; Chapuis, G.; Bünzli, J.-C. G. *Inorg. Chem.* **1988**, *27*, 3518−3526.
(44) Alpha, B.; Ballardini, R.; Balzani, V.; Lehn, J.-M.; Perathoner, S.; Sabbatini, N. *Photochem. Photobiol.* **1990**, *52*, 299−306.

The overall shape of the emission spectra of $[La_{1.96}Eu_{0.04}(L^5)_3]^{6+}$ (**7a**) and $[Gd_{1.96}Eu_{0.04}(L^5)_3]^{6+}$ (**7b**) remains similar with respect to the pure homodinuclear helicate **7** (Figure F7, Supporting Information). Moreover, the intensity of the most intense band ($^5D_0 \rightarrow {}^7F_2$) relative to $^5D_0 \rightarrow {}^7F_1$ is found to be comparable at 77 K while relative intensities of 2.0, 1.7, and 1.6 are recorded for **7**, **7a**, and **7b**, respectively, and the $^5D_0$ level is found to have virtually identical lifetimes at 77 and 295 K for the three compounds (see Table 4). These data point to a series of compounds with very similar structural properties. The emission spectrum of $[Eu_2(L^6)_3]^{6+}$ (**9**) retains essentially the same features as the metal-centered emission from the corresponding compounds with L^5 (Tables 3−5) so it was not studied in detail. These facts, however, allow us to say that the $[Ln_2(L^i)_3]^{6+}$ series of complexes (Ln = La−Gd, i = 5, 6) have solid-state structural properties close to those described for $[Tb_2(L^6)_3]^{6+}$ (**11a**).

The less intense emission spectrum arising from the Tb centers of complex **11** is dominated by the $^5D_4 \rightarrow {}^7F_5$ transition and the relative corrected intensities of the $^5D_4 \rightarrow {}^7F_J$ transitions at 77 K are 1.00, 0.44, 0.53, 0.09, 0.04, and 0.05 for J = 5, 4, 3, 2, 1, and 0, respectively. The lifetime of the $^5D_4$(Tb) state sharply decreases from ca. 2 ms at 77 K to 64 μs at 295 K, which is characteristic of a complex in which a Tb → L^6 energy back-transfer occurs[20,26] as a result of the close proximity in energy of the $^3\pi\pi^*$ state of the ligand (cf. the component at 18 450 cm^{-1} in the emission spectrum of $[Gd_2(L^6)_3]^{6+}$) to the $^5D_4$(Tb) state (18 380 cm^{-1}).

The double-stranded complex $[Eu_2(L^6)_2(CF_3SO_3)_4(H_2O)_2]^{2+}$ (**13**) was also investigated at 10, 77, and 295 K to determine the influence of the coordinated H_2O molecules on the environment of the Eu cation and the lifetime of its $^5D_0$ state. Water is known to decrease significantly the lifetime of the $^5D_0$ state via high-energy OH vibration. The lifetime of the $^5D_0$ state at 77 K (0.76 ms) is typical for a compound where one water molecule is coordinated directly to the Eu(III) ion[1] and is consistent with the crystallographic structure of this compound. Because the lifetime does not decrease significantly in going from 10 to 295 K (0.77 → 0.68 ms), it can be assumed that further luminescence quenching by ligand-to-metal charge transfer states or vibrational quanta from the ligand modes does not occur to a significant extent for this complex. The $^5D_0 \rightarrow {}^7F_0$ excitation spectrum of complex **13** at 77 K produces a single band at 17 239 cm^{-1} with a full width at half-height of 12.2 cm^{-1} (17 248 at 295 K, fwhh = 15.5 cm^{-1}). The ligand excitation band has a maximum at 26 455cm^{-1} and is slightly asymmetrical on the short wavelength side. Excitation through the $^5D_0 \rightarrow {}^7F_0$ metal-based transition or through the ligand band (26 316 cm^{-1}) produces identical spectra displaying crystal field splittings which differ from that of the triple helical complex **7** (Figure F8, Supporting Information). Of particular interest are the patterns of the $^5D_0 \rightarrow {}^7F_1$ and $^5D_0 \rightarrow {}^7F_2$ transitions which suggest a pseudotetragonal symmetry in agreement with the pseudo-monocapped square antiprismatic sites found in the crystal structure of **13a** (Two components A → A and A → E for both $^5D_0 \rightarrow {}^7F_1$ and $^5D_0 \rightarrow {}^7F_2$ transitions, the latter component A → E being split into a doublet).

Solution Properties. Upon complexation, the $\pi \rightarrow \pi^*$ transition of ligands L^5 and L^6 at 43 670 cm^{-1} was observed to undergo a blue shift to approximately 48 700−48 800 cm^{-1} (Table 3) which subsequently revealed a band occurring as a broad shoulder on the $\pi \rightarrow \pi^*$ transition in the free ligand (ca. 41 300 cm^{-1}). The $\pi \rightarrow \pi^*$ transition appearing at longer wavelength (31 200 cm^{-1}) in the free ligand was also observed to shift to lower energies (ca. 29 600 cm^{-1}) on complexation with Ln(III) ions, thus enabling the formation of complexes in solution to be monitored. The spectrophotometric titration of L^5 (10^{-4}−10^{-5} M) with $Ln(ClO_4)_3 \cdot xH_2O$ (Ln = La and Eu) was performed in acetonitrile over M:L^5 ratio in the range 0.1−1.8. The subsequent data displayed inflection points near the Ln:L^5 ratios 0.65 and 1, which would imply the existence of at least two absorbing complex species in solution. This result was confirmed by factor analysis,[27] and the spectrophotometric data were satisfactorily fitted with the equilibria (1) and (2) allowing an estimation of the overall stability constant of each species in solution $\log(\beta_{23}^{La}) = 25.3(9)$, $\log(\beta_{22}^{La}) = 20.4(8)$ and $\log(\beta_{23}^{Eu}) = 24.1(10)$, $\log(\beta_{22}^{Eu}) = 19.9(10)$.

$$2Ln^{3+} + 3L^5 \leftrightarrow [Ln_2(L^5)_3]^{6+} \quad \log(\beta_{23}^{Ln}) \qquad (1)$$

$$2Ln^{3+} + 2L^5 \leftrightarrow [Ln_2(L^5)_2]^{6+} \quad \log(\beta_{22}^{Ln}) \qquad (2)$$

The use of electrospray mass spectrometry (ES-MS) to characterize qualitatively the distribution of preformed ions in solution has been well documented[16,29,30] and has been employed by us for this purpose on previous occasions.[23−26] Solutions of Ln(III) and L^5 (Ln = La and Eu) with a total L^5 concentration of 10^{-4} M are prepared under the following stoichiometric conditions: 1:3, 2:3, 1:1, and 3:2 Ln/L^5. Relevant data are reported in Table 6. At low Ln(III) ion concentration (1:3 Ln/L^5) complicated spectra are observed in which peaks assigned to the protonated free ligand $[L^5 + H]^+$ (*m/z* 629.2) and the $[Ln_2(L^5)_3]^{6+}$ cations and their perchlorate adducts[30] are detected. As the concentration of Ln(III) ion is increased (2:3 Ln/L^5, Figure 6), the spectra simplify and only the 2:3 species $[Ln_2(L^5)_3]^{6+}$ cations and their perchlorate adducts $[Ln_2(L^5)_3(ClO_4)_i]^{(6-i)+}$ are in evidence. The peaks of the 2:3 complex still dominate the spectra in the presence of excess of metal ion because unsaturated lanthanide complexes where solvent molecules are coordinated to Ln(III) are known to possess large solvation energies and weak ES-MS responses.[23,24] However, $[Ln_2(L^5)_2(ClO_4)_i]^{(6-i)+}$ cations (i = 3, 4) are also detected as minor peaks which demonstrates the formation of 2:2 complexes for Ln:$L^5 \geq 1.0$. These data qualitatively confirm the preferential formation of the dinuclear triple-stranded helicate by a self-assembly process as well as the speciation established by the spectrophotometric study which foresees the conversion of the 2:3 complex $[Ln_2(L^5)_3]^{6+}$ into the 2:2 complex $[Ln_2(L^5)_2]^{6+}$ in excess of metal.

Table 6. Molecular Peaks of Main La and Eu Complexes and Adduct Ions Observed by ES-MS Employing the Ln:L^5 Ratio Indicated

species	*m/z*	obsd for Ln:L^5 ratios			
	Ln = Eu				
$[Eu_2(L^5)_2(ClO_4)_4]^{2+}$	979.2				3:2
$[Eu_2(L^5)_2(ClO_4)_3]^{3+}$	619.7				3:2
$[Eu_2(L^5)_3(ClO_4)_4]^{2+}$	1293.3	1:3	1:1	2:3	3:2
$[Eu_2(L^5)_3(ClO_4)_3]^{3+}$	829.3	1:3	1:1	2:3	3:2
$[Eu_2(L^5)_3(ClO_4)_2]^{4+}$	597.1	1:3	1:1	2:3	3:2
$[Eu_2(L^5)_3(ClO_4)]^{5+}$	457.8	1:3	1:1	2:3	3:2
$[Eu_2(L^5)_3]^{6+}$	365.1	1:3	1:1	2:3	
	Ln = La				
$[La_2(L^5)_2(ClO_4)_4]^{2+}$	966.2		1:1[a]		3:2
$[La_2(L^5)_3(ClO_4)_4]^{2+}$	1280.6	1:3	1:1	2:3	3:2
$[La_2(L^5)_3(ClO_4)_3]^{3+}$	820.6	1:3	1:1	2:3	3:2
$[La_2(L^5)_3(ClO_4)_2]^{4+}$	590.6	1:3	1:1	2:3	3:2
$[La_2(L^5)_3(ClO_4)]^{5+}$	452.6	1:3	1:1	2:3	3:2
$[La_2(L^5)_3]^{6+}$	360.7		1:1	2:3	3:2

[a] Minor species.

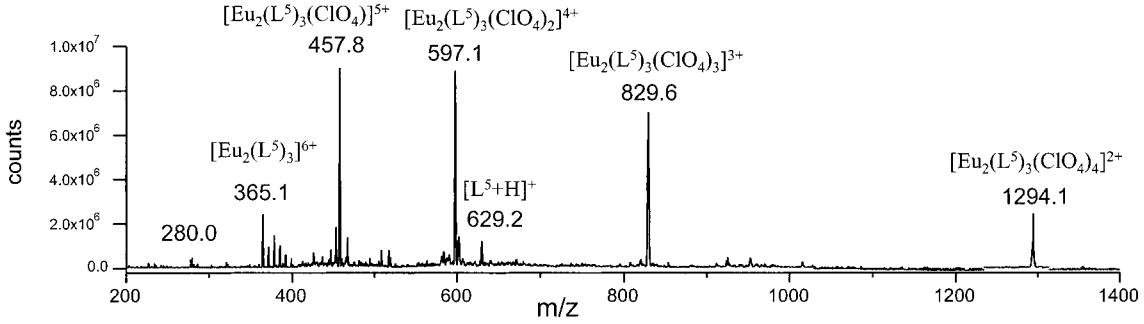

Figure 6. ES-MS spectrum of a solution of 10^{-4} M Eu(III) and L^5 in anhydrous acetonitrile with a Eu:L^5 ratio of 2:3.

Table 7. ^{1}H-NMR Shifts (with Respect to TMS) for L^5 and L^6 and Their Complexes in CD_3CN at 298 K

	H^1	H^2	H^3	H^4	H^6	H^7	H^8	$H^{9,10}$	$H^{11,12}$	Me^2	Me^3
L^5	4.11	7.67	7.14	7.49	8.32	8.15	7.34	3.58	3.34	1.21	1.06
$[La_2(L^5)_3]^{6+}$ (**6**)	3.62	5.99	7.25	7.53	8.41	8.20	7.63	2.91, 2.91	3.24, 3.42	0.93	0.71
$[Eu_2(L^5)_3]^{6+}$ (**7**)	4.43	13.5	7.69	6.40	4.75	6.23	5.09	2.84, 3.91	2.56, 3.12	3.31	0.61
L^6	4.2	7.65	7.27	7.5	8.35	8.01	7.50	3.55	3.34	1.22	1.05
$[La_2(L^6)_3]^{6+}$ (**8**)	3.74	6.07	7.49	7.21	8.3	8.2	7.73	3.42, 3.71	2.69, 3.06	1.07	0.8
$[Eu_2(L^6)_3]^{6+}$ (**9**)	4.47	12.9	7.69	6.41	4.93	6.4	5.27	2.67, 4.03	2.67, 3.85	3.45	0.73
$[Lu_2(L^6)_3]^{6+}$ (**12**)	3.64	5.52	7.12	7.43	8.45	8.2	7.69	4.70, 4.79	2.67, 2.75	0.63	1.13

For Ln:L^5 = 0.67 and a total concentration of ligand of 0.015 M, $[Ln_2(L^5)_3]^{6+}$ is the only complex (>95% of ligand speciation) in acetonitrile (eqs 1 and 2). The well-resolved ^{1}H-NMR spectra observed for the diamagnetic complexes of $[Ln_2(L^6)_3]^{6+}$ (Ln = La and Lu) and $[La_2(L^5)_3]^{6+}$ in acetonitrile at ambient temperature reflect the stability and the dynamic inertness of these self-assembled cations in solution and also implies that the triple helical structure adopted by the cation in the solid state (cf. the X-ray crystal structure of $[Tb_2(L^6)_3]^{6+}$) is maintained in solution (Table 7). That is to say, the ^{1}H-NMR of these diamagnetic complexes displays features which typifies a cation possessing a triple helical pseudo-D_3 symmetry; namely, the bridging methylene protons $H^{1a,1b}$ remain enantiotopic while $H^{9,10}$ and $H^{11,12}$ display AB spin systems as a result of their diastereotopic relationship upon complexation.[26,45] The signals arising from the aromatic protons in the range 5−8.5 ppm were observed to undergo significant shifts relative to the corresponding signals in the free ligand with the most notable (upfield) shift detected for the aromatic proton H^2. This has been explained, after examination of the crystal structure of the $[Tb_2(L^6)_3]^{6+}$ cation, to originate from the combination of shielding effects arising from the benzimidazole ring connected to the methylene spacer (intrastrand: typical for helically twisted strands)[46] and the aromatic benzimidazole rings belonging to the two other strands of the triple helix (interstrand).[26] As a consequence of the perturbation of the aromatic field by the positively charged ion, the pyridine (H^6, H^7, H^8) signals show the expected downfield shift on complexation.[20] Due to the increased electrostatic interaction, an enhancement of this effect is detected for $[Lu_2(L^6)_3]^{6+}$. Although the general character of the ^{1}H-NMR spectra is maintained for the La and Lu analogs of L^6, the upfield shift of H^2 observed for the Lu helicate suggests a small distortion of the coordination sphere arising from the contraction of the Ln(III) radii.[23] Many of the features depicted in the ^{1}H-NMR spectra of the diamagnetic cations of these systems were also observed for the paramagnetic $[Eu_2(L^5)_3]^{6+}$ and $[Eu_2(L^6)_3]^{6+}$ cations (enantiotopic $H^{1a,1b}$ and diastereotopic $H^{9,10}$ and $H^{11,12}$ protons); however, due to the coupling between the electronic and nuclear magnetic moments of the paramagnetic Eu(III) center and the protons of the ligands, the signal arising from H^2 was perceived to undergo broadening and a significant downfield shift of approximately 5.6 ppm in the ^{1}H-NMR spectra of both Eu(III) triple-stranded helicates.[24,47]

Further investigations into size discriminatory effects of L^5 between La and Eu were carried out. A sample containing 3 equiv of L^5, 1 equiv of $La(ClO_4)_3 \cdot 4.6H_2O$, and 1 equiv of $Eu(ClO_4)_3 \cdot 6.7H_2O$ was prepared in acetonitrile, evaporated, and dried under high vacuum for 24 h before redissolving in CD_3CN. The aromatic region of the ^{1}H-NMR spectrum of the resultant solution is depicted in Figure F9 (Supporting Information). An analysis based on comparison of the aromatic region of the ^{1}H-NMR spectra of the homodinuclear Eu and La complexes allows one to assign signals in this region. The presence of the paramagnetic Eu(III) ion results in the signal arising from H^2 appearing at low field for both the homodinuclear and the Eu end of the heterodinuclear complexes, and one can estimate using the integrals of the corresponding ^{1}H-NMR signals a distribution of the complexes: 25% of homodinuclear species for each ion and 50% heterodinuclear species in solution. This statistical formation of the heterodinuclear complex for the Eu/La pair has been previously reported for L^4 and due to the unchanging nature of the spectra over a period of weeks was described as a thermodynamic rather than kinetic effect.[26] It is in line with the log β_{23} values determined by spectrophotometry for La and Eu which are not statistically different.

Finally, we have examined the luminescence properties of the dinuclear triple-stranded helicates $[Ln_2(L^5)_3]^{6+}$ (Ln = Eu, Tb) 10^{-3} M in anhydrous acetonitrile. Excitation through the ligand level (385 nm) results in an emission spectrum which, despite being relatively broad with fewer maxima than observed in the solid state, is typical of the metal-based f → f transitions of these metal ions. Although site symmetry determination is prohibited by the broad nature of the Eu emission bands in solution, their general features strongly suggest that the pseudo-trigonal arrangement is maintained. Encouraged by the increased protection offered to the included Eu ion by the terminal

(45) Rüttimann, S.; Piguet, C.; Bernardinelli, G.; Bocquet, B.; Williams, A. F. *J. Am. Chem. Soc*. **1992**, *114*, 4230−4237.
(46) Piguet, C.; Hopfgartner, G.; Bocquet, B.; Schaad, O.; Williams, A. F. *J. Am. Chem. Soc.* **1994**, *116*, 9092−9102.
(47) Bertini, I.; Luchinat, C. *NMR of Paramagnetic Molecules in Biological Systems*; Benjamin/Cummings Publishing Co. Inc.: Menlo Park, CA, 1986; Chapter 10.

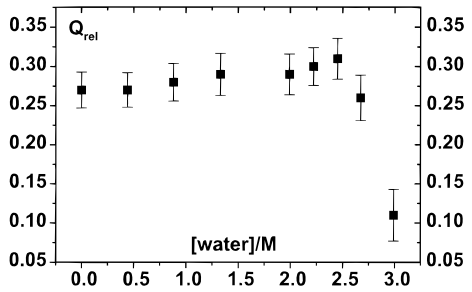

Figure 7. Quantum yield relative to $[Eu(terpy)_3]^{3+}$ for solutions of 10^{-3} M $[Eu_2(L^5)_3]^{6+}$ in acetonitrile, measured versus concentration of added water.

Table 8. Quantum Yields (Q_{rel}, ±10%) at 295 K of Anhydrous Acetonitrile Solutions of $[Ln_2(L^i)_3]^{6+}$ ($i = 4, 5$) Relative to $[Eu(terpy)_3]^{3+}$ (terpy = 2,2′:6′,2″-Terpyridine)

compd	10^3·conc of compd (M)	conc of H_2O (M)	λ_{exc} (nm)	$\epsilon(\lambda_{exc})$ (M^{-1}·cm^{-1})	Q_{rel}
$[EuZn(L^2)_3]^{5+}$ [a]	1	0	442	530	$\approx 1 \times 10^{-4}$
$[EuZn(L^3)_3]^{5+}$ [a]	1	0	395	555	0.13
$[Eu(terpy)_3]^{3+}$	1.2	0	367	310	1
$[Eu_2(L^5)_3]^{6+}$	1.1	0	397	482	0.27
		2.45		373	0.31
		2.99		291	0.11
$[Eu_2(L^4)_3]^{6+}$	1.1	0	440	367	5.1×10^{-3}
$[Tb(terpy)_3]^{3+}$	1.2	0	367	328	1
$[Tb_2(L^5)_3]^{6+}$	1.2	0	394	308	0.28

[a] Taken from ref 24.

carboxamide unit with respect to the benzimidazole group reported for Eu complexes of ligands L^2 and L^3,[23] we have performed an analogous quantum yield determination with L^5. For a 10^{-3} M solution of complex **7**, we calculate that $[Eu_2(L^5)_3]^{6+}$ corresponds to 80% of the metal speciation (eqs 1 and 2), which precludes measurements at lower concentrations even though more accurate data are generally obtained under more diluted conditions. The quantum yield relative to $[Eu(terpy)_3]^{3+}$ at the same concentration is $Q_{rel} = 0.27$, which can be compared to the poor luminescence of the analogous helicate $[Eu_2(L^4)_3]^{6+}$ ($Q_{rel} = 0.005$) determined under the same experimental conditions. Upon addition of H_2O up to a concentration of 2.5 M (which translates to $\approx 2 \times 10^3$ fold excess of H_2O), a slight nonsignificant increase from 0.27 to 0.31 in relative quantum yield was observed (see Table 8 and Figure 7). The addition of more water resulted in a drastic decrease in relative quantum yield due to probable dissociation of the complex. Nonetheless we can report a 54-fold increase in relative quantum yield over that measured for the analogous $[Eu_2(L^4)_3]^{6+}$ helicate and a significant improvement in resistance to hydrolysis over the latter complex where 0.2 M addition of H_2O resulted in complete quenching of the metal-based luminescence. For the reference $[Eu(terpy)_3]^{3+}$ complex, a 63% reduction of luminescence intensity was noticed upon addition of 0.93 M H_2O.[24]

Discussion

The crystal structures of compounds **11a** and **13a** show a stark contrast in the architectures adopted during their self-assembly revealing a dependence on the counterion employed during the synthesis. Although both are dinuclear with a similar intermetallic distance (ca. 9.05 Å) and with each ion lying in nine-coordinate sites, the $[Tb_2(L^6)_3]^{6+}$ complex formed in the presence of the ClO_4^- counterion is bound to three ligands twisted in a triple helical architecture while the $[Eu_2(L^6)_2(CF_3SO_3)_4(H_2O)_2]^{2+}$ complex formed from the $CF_3SO_3^-$ salt possesses only two strands adopting a side-by-side arrangement leading to a nonhelical C_{2h} double-stranded helicate. To the best of our knowledge,[16] this is the first documented assembly of double- and triple-stranded dinuclear helicates obtained from the same components but controlled by the choice of the poorly coordinating anion.[48] This observation suggests that the self-assembly process leading to the final lanthanide helicates possesses a rather flat energy hypersurface which is confirmed by the ES-MS, ^{1}H-NMR, and spectrophotometric data showing the successive formation of the D_3-helical triple-stranded helicate $[Ln_2(L^6)_3]^{6+}$ and the 2:2 complex $[Ln_2(L^6)_2]^{6+}$ in solution. According to the crystal structures of **11a** and **13a**, the conversion of $[Eu_2(L^6)_3]^{6+}$ into $[Eu_2(L^6)_2(CF_3SO_3)_4(H_2O)_2]^{2+}$ is associated with the unfolding of the strands which is expected to be favored by the negligible π-stacking interactions exhibited in **11a**. A related behavior has been reported for the mononuclear triple helical complexes $[Ln(L^1)_3]^{3+}$ which produces only 1:2 complexes with the small Lu(III).[17] However, the strong interstrand stacking interactions found in these complexes and the rigidity of the tridentate aromatic units prevent the unfolding of the strands whose helicity is retained in $[Lu(L^1)_2(CH_3OH)(H_2O)_2]^{2+}$.[17,18] We conclude that the wrapping of the three strands in $[Tb_2(L^6)_2]^{6+}$ seems to be essentially governed by the strong ion−dipole interactions. As observed in $[EuZn(L^3)_3]^{5+}$ [24] and $[Eu_2(L^4)_3]^{6+}$,[26] aromatic $\pi-\pi$ interactions seemingly play no role in maintaining the helical edifice, while they are of considerable strength in $[Eu(L^1)_3]^{3+}$.[17]

A careful comparison between the IR spectra of the Eu and Tb complexes with L^5 shows that these compounds are very similar in nature and suggests that the structure of the Eu compound resembles that of the structurally determined $[Tb_2(L^6)_3]^{6+}$ complex. Moreover, the crystal field splittings evident from the emission spectra of the $[Eu_2(L^i)_3]^{6+}$ ($i = 5, 6$) compounds are alike and consistent with the previous evidence. The long lifetimes of the Eu($^5D_0$) level in $[Eu_2(L^i)_3]^{6+}$ ($i = 5, 6$) indicates that the Eu(III) ions are well protected by the helical ligands from solvent interaction (Table 4), as confirmed by the quantum yield determination in presence of water. The ligand to lanthanide energy transfer was found to be efficient for Eu(III) and goes through the $^3\pi\pi^*$ state; the energy difference $\Delta E(^3\pi\pi^*\text{-Eu}^*)$ is ca. 3700 and 1900 cm^{-1} for $^5D_0$ and $^5D_1$, respectively, taking into account the 0-phonon transition of the ligand triplet state as measured for $[Gd_2(L^6)_3]^{6+}$. These values are close to the optimum differences reported in recent papers.[49,50] From their work on sensitizer-modified calix[4]arenes, Reinhoudt and co-workers conclude that the 0-phonon band of the ligand triplet state must be 3500 cm^{-1} above the Ln excited state to ensure efficient energy transfer.[49] In another investigation, Latva[50] has determined the luminescence quantum yields of 41 Eu and Tb chelates as a function of the $^3\pi\pi^*$ 0-phonon transition of the ligand and reaches a similar conclusion, the best efficiency in energy transfer being obtained when this component lies around $(21-22) \times 10^3$ cm^{-1}. With respect to L^4, the presence of the terminal carboxamide unit explains this beneficial influence on the luminescent properties of the Eu ion for the following reasons: (i) The temperature-independent lifetime of the $^5D_0$ state of $[Eu_2(L^i)_3]^{6+}$ ($i = 5, 6$)

(48) Bünzli, J.-C. G.; Merbach, A .E.; Nielson, R. M. *Inorg. Chim. Acta* **1987**, *139*, 151−152.
(49) Steemers, F. J.; Verboom, W.; Reinhoudt, D. N.; Vandertol, E. B.; Verhoeven, J. W. *J. Am. Chem. Soc.* **1995**, *117*, 9408−9414.
(50) Latva, M.; Takalo, H.; Mukkala, V. M.; Matachescu, C.; Rodriguez-Ubis, J. C.; Kankare, J. *J. Lumin.* **1997**, *75*, 149−169. Latva, M.; Takalo, H.; Mukkala, V. M.; Kankare, J. *Inorg. Chim. Acta* **1998**, *267*, 63−72.

suggests a blue shift of the LMCT level with respect to the $[Eu_2(L^4)_3]^{6+}$ helicate, where a sharp decrease in the lifetime on going from 150 to 295 K was observed. (ii) The shorter Ln−O bonds with respect to the Ln−N bonds provide a more rigid environment for the Eu ion and therefore favor radiative deexcitation evident from the long lifetimes and intense luminescence of $[Eu_2(L^i)_3]^{6+}$ ($i = 5, 6$) complexes at ambient temperature. (iii) We have previously reported that the ν(C═O) bond may facilitate deexcitation of the Eu($^5D_1$) level to Eu($^5D_0$), the energy difference corresponding to one ν(C═O) phonon.[51] (iv) The reduced number of close interstrand contacts between the wrapped aromatic rings in $[Eu_2(L^i)_3]^{6+}$ ($i = 5, 6$) compared to $[Eu_2(L^4)_3]^{6+}$ limits the formation of excimer states.[17,21] In contrast, the Tb-based emission originating from the $[Tb_2(L^6)_3]^{6+}$ helicate displays a significantly lower intensity with respect to the Eu-centered emission from $[Eu_2(L^i)_3]^{6+}$ and the short lifetime of the Tb($^5D_4$) state displays a notable temperature dependence. This is consistent with a compound in which the close proximity of the Tb excited levels and the ligand $^3\pi\pi^*$ state leads to a situation unfavorable for energy transfer and favorable for energy back-transfer from the Tb($^5D_4$) state to the ligand levels. According to Latva,[50] back-transfer occurs when $\Delta E(^3\pi\pi^*$-Tb*) is less than 1850 cm^{-1}, which again is the case for $[Tb_2(L^6)_3]^{6+}$ (ca. 500 cm^{-1}).

A correlation between the energy of the Eu($^5D_0 \rightarrow {}^7F_0$) transition, that is the position of the $^5D_0$ level, and parameters describing the ability δ of coordinating atoms to produce a nephelauxetic effect has been recently proposed:[52] $\tilde{\nu} - \tilde{\nu}_0 = C_{CN}\sum_i n_i\delta_i$, where C_{CN} is a coefficient depending upon the Eu^{III} coordination number (1.0 for CN = 9; 0.95 for CN = 10), n_i is the number of atoms of type i, and $\tilde{\nu}_0 = 17\,374$ cm^{-1} at 295 K. The parameters δ have been tabulated for several functional groups.[52] We have demonstrated that a heterocyclic N-atom (HN) tends to produce a larger nephelauxetic effect than an amine N-atom (−12.1)[52] and have deduced from our work on 9-coordinate triple-helical complexes with monotopic and ditopic ligands based on bis(benzimidazolyl)pyridines a δ_{HN} parameter equal to −15.3.[21,23,24] Taking the latter value into account, as well as $\delta_{CO} = -15.7$ and $\delta_{OH} = -11.6$,[52] we derive $\delta_{triflate} = -10.7$ from the observed $^5D_0 \rightarrow {}^7F_0$ transition in the $[Eu_2(L^6)_2(CF_3SO_3)_4(H_2O)_2]^{2+}$ cation. This value is in line with the weak Eu−triflate interaction[48] since the nephelauxetic parameters for nitrate ($\delta_{O(NO3)} = -13.3$)[52] and for carboxylate ($\delta_{OOCR} = -17.2$)[52] are substantially larger. This relationship is to be used with care since the δ parameters are very sensitive to bonding distances and, probably, to the conformation of the ligand.[50] For $[Eu_2(L^6)_3]^{6+}$ we have to take into account the three metal ion sites evidenced (Figure 5) and to allow for a temperature correction (1 cm^{-1} per 24 K, that is +9 cm^{-1} in going from 77 to 295 K);[53] we find 17 219 (site Ia), 17 233 (site Ib), and 17 245 cm^{-1} (site II) while calculation with the above-mentioned parameters yields 17 235 cm^{-1}. The discrepancies observed for sites Ia and II may be rationalized in terms of Eu−X bonding distances since the crystal structure of the Tb helicate has revealed one environment (Tb(1)) with shorter bonding distances than the other one (Tb(2)). The Tb−X distances also span a wide range, reflecting nonsymmetrical bonding, which renders more difficult the assignment of a single δ parameter for each ligating group. For site II, outer-sphere interaction between water and the ligand strands may weaken the Eu−L^6 bonding, resulting in a lower δ parameter.

Finally, ^{1}H-NMR and ES-MS data imply that $[Eu_2(L^i)_3]^{6+}$ ($i = 5, 6$) retain their triple-helical structure in solution as similarly found for $[Eu_2(L^4)_3]^{6+}$.[26] Quantum yield measurements display an improved luminescence for $[Eu_2(L^5)_3]^{6+}$ and a good resistance toward hydrolysis which implies that the terminal carboxamide unit provides a more rigid metal environment than either the terpy ligand or L^4. Furthermore, assuming that $[Eu_2(L^5)_3]^{6+}$ adopts an architecture isomorphous to that of $[Tb_2(L^6)_3]^{6+}$, comparative examination of the crystal structures of the $[Tb_2(L^6)_3]^{6+}$ and $[Eu_2(L^4)_3]^{6+}$ [26] helicates reveals that the Eu(III) ion is considerably more shielded from external interaction by the carboxamide than the benzimidazole group which may prevent the introduction of solvent molecules into the internal coordination sphere and consequently the radiationless deexcitation processes associated with solvent interaction.

Conclusion

If one takes into account the *induced fit concept*, two acyclic ligands which present both homogeneous (three amine functions) and nonhomogenous (two amine and one amide functions) tridentate donor sets coded for selective coordination of Ln(III) ions have been designed and synthesized. The intrinsic advantages afforded by the flexible synthetic route employed to isolate this series of podands results in a certain degree of fine structural control not easily attained by lengthy procedures involved in the synthesis of conventional cyclic or polycyclic receptors. Subsequently, structural tailoring of the coordination site can lead to enhancement of the stability and luminescent properties of the complexes of these ligands. The thermodynamic self-assembly of L^{5,6} with Ln(III) produces two successive dinuclear complexes. The expected D_3-helical triple-stranded helicate $[Ln_2(L^i)_3]^{6+}$ ($i = 5, 6$) is formed for a stoichiometric ratio Ln:L^i = 0.67, while excess of metal ion led to the solvated 2:2 complex $[Ln_2(L^i)_2]^{6+}$. Its isolation in the solid state definitely establishes its existence as a dinuclear C_{2h} side-by-side double-stranded helicate. A related behavior has been invoked in the literature only once for the poorly characterized double- ($n = 2$) and triple-stranded ($n = 3$) helicates $[Zn_2(L^7)_n]^{4+}$ observed for the titration of L^7 with $Zn(ClO_4)_2 \cdot 6H_2O$.[33] The coexistence of significant quantities of both complexes $[Ln_2(L^5)_3]^{6+}$ and $[Ln_2(L^5)_2]^{6+}$ in solution for the stoichiometric Ln:L^5 ratio in the range 0.5−1.0 according to eqs 1 and 2 suggests that a negative cooperative process occurs,[54] which contrasts with the positive cooperativity demonstrated by Lehn and coworkers for trinuclear double-stranded copper(I) helicates.[55] We suspect that the larger charge borne by the Ln(III) compared to Cu(I) is responsible for higher coulombic repulsion in the resulting dinuclear complexes which may explain the different behavior in the assembly process. However $[Ln_2(L^i)_3]^{6+}$ ($i = 5, 6$) are sufficiently stable to be selectively produced in solution under suitable stoichiometric conditions in acetonitrile. Although on one hand L$^{4-6}$ present structurally and photophysically similar coordination sites for Ln(III) ions, we have demonstrated on the other hand that the carboxamide moiety significantly alters the electronic properties of the tridentate binding unit, resulting in a significant enhancement of the metal-centered luminescence in $[Eu_2(L^i)_3]^{6+}$ ($i = 5, 6$) and in an improved resistance toward hydrolysis over that observed for the helicate with L^4 which possesses benzimidazole terminal

(51) Bünzli, J.-C. G.; Yersin, J.-R. *Helv. Chim. Acta* **1982**, *65*, 2498−2506.
(52) Frey, S. T.; Horrocks, W. deW., Jr. *Inorg. Chim. Acta* **1995**, *229*, 384−390.
(53) Albin, M.; Horrocks, W. deW., Jr. *Inorg. Chem.* **1985**, *24*, 895−900.
(54) Perlmutter-Hayman, B. *Acc. Chem. Res.* **1986**, *19*, 90−96.
(55) Garrett, T. M.; Koert, U.; Lehn, J.-M. *J. Phys. Org. Chem.* **1992**, *5*, 529−532. Pfeil, A.; Lehn, J.-M. *J. Chem. Soc., Chem. Commun.* **1992**, 838−840.

groups. Consequently these encouraging results bring the goal of tailored luminescent probes and nanometric light-converting devices with predetermined physicochemical properties within the realms of possibility.

Acknowledgment. We gratefully acknowledge Ms. Véronique Foiret and Mr. Hugues Siegenthaler for technical assistance. C.P. thanks the Werner Foundation for a fellowship, and J.-C.G.B. thanks the Fondation Herbette (Lausanne, Switzerland) for the gift of spectroscopic equipment. This work is supported through grants from the Swiss National Science Foundation.

Supporting Information Available: Tables for elemental analyses and IR data for the complexes, tables of crystal data, atomic coordinates, isotropic and anisotropic displacement parameters, and bond lengths and angles for $[Tb_2(L^6)_3](ClO_4)_6(THF)_{0.5}(MeCN)_2(EtOH)_{0.5}$ (**11a**) and $[Eu_2(L^6)_2(CF_3SO_3)_4(H_2O)_2](CF_3SO_3)_2(MeOH)_2(H_2O)_{5.5}$ (**13a**), a table listing the relative intensities of the $^5D_0 \rightarrow {}^7F_J$ transitions, and figures showing thermal ellipsoids and packing diagrams for **11a** and **13a** and reflectance, excitation and emission, and NMR spectra of various complexes (41 pages). Ordering information is given on any current masthead page.

IC971401R